Towards Data Driven Stamping Process Modelling by Optical Inline Monitoring of Cutting Surface Parameters

Maximilian Lorenz (maximilian.lorenz@hs-kempten.de)
University of Applied Science Kempten https://orcid.org/0000-0001-7443-861X
Matthias Menzl
Hochschule Kempten
Christian Donhauser
University of Applied Sciences Kempten: Hochschule Kempten
Michael Layh
Hochschule fur angewandte Wissenschaften Kempten: Hochschule Kempten
Bernd R. Pinzer
University of Applied Sciences Kempten: Hochschule Kempten

Research Article

Keywords: inline optical inspection, quality control, process data, predictive maintenance, stamping

Posted Date: April 8th, 2021

DOI: https://doi.org/10.21203/rs.3.rs-376983/v1

The International Journal of Advanced Manufacturing Technology

Title Page

Names of the authors:
Maximilian Lorenz, Matthias Menzl, Christian Donhauser, Michael Layh, Bernd R. Pinzer

Title:
Towards data driven stamping process modelling by optical inline monitoring of cutting surface parameters

Affiliation and address of the authors:
University of Applied Sciences Kempten, Bahnhofstrasse 61, 87435 Kempten, Germany

E-mail address of the corresponding author: Maximilian.Lorenz@hs-kempten.de

ORCID of corresponding author: https://orcid.org/0000-0001-7443-861X

Abstract:
Stamping is a wide-spread production process, applied when massive amounts of the ever-same cheap parts are needed. For this reason, a highly efficient process is crucial. The cutting process is sensitive to a multitude of parameters. A process that is not correctly adjusted is subject to considerable wear and therefore not efficient. Unfortunately, the precise dependencies are often unknown. A prerequisite for optimal, reproducible and transparent process alignment is the knowledge of how exactly parameters influence the quality of a cutting part, which in turn requires a quantitative description of the quality of a part. A data driven approach allows to meet this challenge and quantify these influences.
We developed an optical inline monitoring system, which consists of a image capturing, triangulation and image processing, that is capable of deriving quality metrics from 2D images and triangulation data of the cutting surface, directly inside the machine and without affecting the process. We identify features that can be automatically turned into quality metrics, like fraction of the burnish surface or the cut surface inclination.
As an application, we show that the status of tool wear can be inferred by monitoring the burnish surface, with immediate consequences for predictive maintenance. Furthermore, we conclude that connecting machine and process parameters with quality metrics in real time for every single part enables data driven process modelling and ultimately the implementation of intelligent stamping machines.

Keywords:
inline optical inspection, quality control, process data, predictive maintenance, stamping

Declarations:

Funding:
The Authors gratefully acknowledge financial support from the interdisciplinary technology network Efficient Production Technology (EffPro), co-funded by the European Union and the Free State of Bavaria from the European Fund for regional development (ERDF) and supported by the University of Applied Sciences Kempten and the Bavarian Ministry of Science and Art.

Conflicts of interest:
The authors declare that they have no conflict of interest.

Availability of data and material:
The data that support the findings of this study are available from the corresponding author on reasonable request.

Code availability:
For Image processing a custom code was implemented in Python. The Software GOM Inspect (Freeware) and CouldCompare(GNU) were used for 3D-Data comparison.

The International Journal of Advanced Manufacturing Technology manuscript No.
(will be inserted by the editor)

Towards data driven stamping process modelling by optical inline monitoring of cutting surface parameters

Maximilian Lorenz · Matthias Menzl · Christian Donhauser · Michael Layh · Bernd R. Pinzer

Received: date / Accepted: date

Abstract Stamping is a wide-spread production process, applied when massive amounts of the ever-same cheap parts are needed. For this reason, a highly efficient process is crucial. The cutting process is sensitive to a multitude of parameters. A process that is not correctly adjusted is subject to considerable wear and therefore not efficient. Unfortunately, the precise dependencies are often unknown. A prerequisite for optimal, reproducible and transparent process alignment is the knowledge of how exactly parameters influence the quality of a cutting part, which in turn requires a quantitative description of the quality of a part. A data driven approach allows to meet this challenge and quantify these influences.
We developed an optical inline monitoring system, which consists of an image capturing, triangulation and image processing, that is capable of deriving quality metrics from 2D images and triangulation data of the cutting surface, directly inside the machine and without affecting the process. We identify features that can be automatically turned into quality metrics, like fraction of the burnish surface or the cut surface inclination.
As an application, we show that the status of tool wear can be inferred by monitoring the burnish surface, with immediate consequences for predictive maintenance. Furthermore, we conclude that connecting machine and process parameters with quality metrics in real time for every single part enables data driven process modelling and ultimately the implementation of intelligent stamping machines.

Keywords inline optical inspection · quality control · process data · predictive maintenance · stamping

Maximilian Lorenz
Laboratory for Optical 3D Metrology and Computer Vision
University of Applied Sciences Kempten
87435 Kempten, Germany
E-mail: maximilian.lorenz@hs-kempten.de

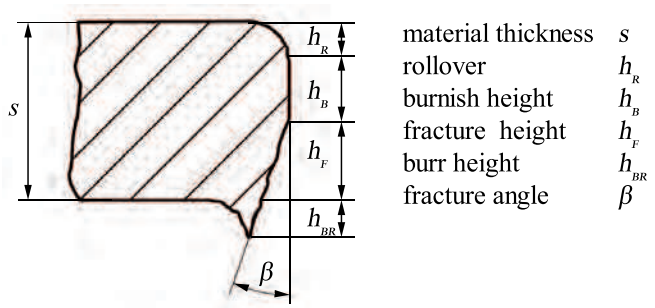

Fig. 1: Definition of the cutting surface parameters [6]

1 Introduction

Stamping and blanking are manufacturing processes for the mass production of high quality and economical parts especially for the automotive industry and electronic contact elements [1]. The cutting surface can often be used directly as a functional surface. A high proportion of the burnish surface is desired. We therefore regard the burnish height (h_B) to be the quality and process-determining factor [2, 3, 4, 5]. A surface with a higher percentage of burnish height represents a higher quality. Other quality indicators defined in the literature are the rollover, fracture height and burr height [6], see Figure 1. We collectively refer to these parameters as "cutting surface parameters". Attempts to optimize the quality of stamping parts with respect to cutting surface parameters are currently based exclusively on expert knowledge and the trial-and-error method. This is due to the fact that there are many factors influencing the process in unknown ways; examples are shown in Figure 2. Moreover, the wide variety of machine-, tool-, material- and process-parameters and their mutual dependencies render it very difficult to compare the results of different process studies. [3, 7, 8]

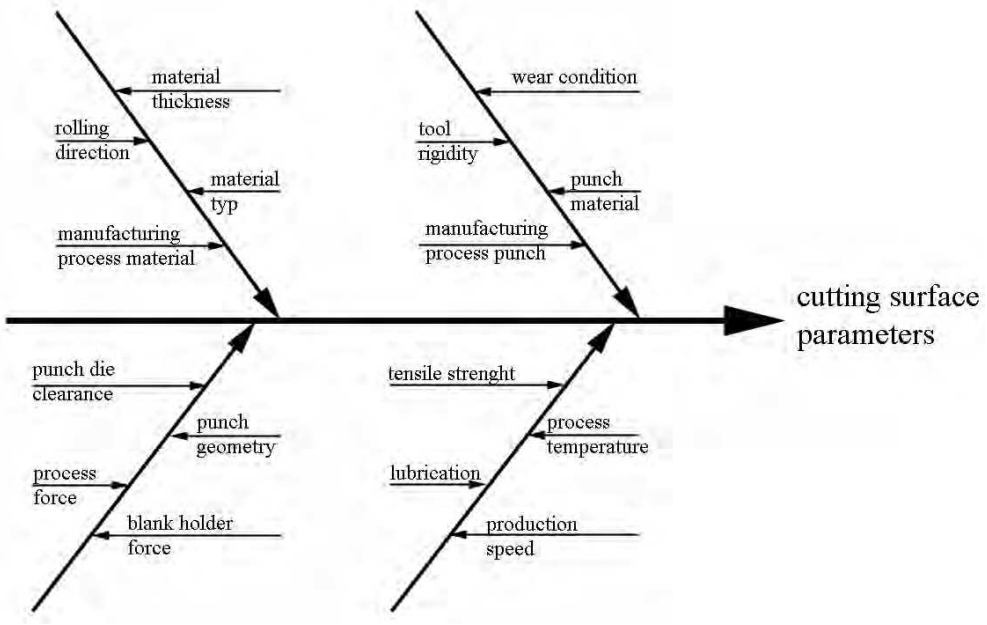

Fig. 2: Selection of process parameters that are most likely to influence the cutting surface parameters

The influence of these process parameters, lack of an accurate prediction of material separation and rigidity requirements from the process also complicate the design and dimensioning of the stamping tool [9, 8]. Therefore, the tool designs are based on the empiric model in [10]. In this model, the maximum process force $F_{s,max}$ is calculated according to

$$\begin{aligned} F_{s,max} &= l \cdot s \cdot k_s \\ k_s &= c \cdot R_m, \end{aligned} \tag{1}$$

where l is the punch circumference in mm, s is the material thickness in mm, and k_s is an empirical factor called the specific cutting force parameter in N/mm. k_s depends on the tensile strength R_m of the material and a parameter c in the range from 0.6 to 0.9 [10, 11]. The parameter c is interpreted as a *correction factor*, which combines all variations of the process parameters for example cutting length, ratio between cutting area and material thickness. In practice the maximum process force $F_{s,max}$ often differs $\pm 20\%$ from this model. [10] Parameters variations lead to deviations within the cutting surface parameters and change of h_B. A key indicator is the wear of the punch. It is correlated with the quality of the produced parts [12]. A new punch has a well defined edge radius. A worn punch shows blow outs along its edge. This effect is similar to an increased cutting edge radius [13]. This results in a higher punch-die clearance[5] and could increase the process force and the quality of the cutting surface [14]. As summarized by [15, 3, 16] the process is still not fully captured by any comprehensive process model. Different experiments with different parameters show either an increase or a decrease in the cutting edge/surface parameters and thus come to contradictory conclusions; the high-dimensional parameter space renders comparison and interpretation of the results very difficult.

Numerous studies have investigated the influence and correlations of these parameters with the quality of the stamping parts. In addition some studies use measured process parameters (e.g. acceleration [17], force [18], acoustic emission [19]) to indirectly describe the quality of the stamping parts. Monteil et. al.[20] developed a method for in situ punch wear measurement. A thin layer activation is performed on the punch surface. The worn volume can be measured by the activity of the punch after a certain interval. The machine must be stopped and a probe must be placed underneath the punch. Also process-driven feature engineering approaches where presented. Mardapittas et. al. [21] presented an expert system for tool condition monitoring. An acoustic emission sensor, an optical signal for detection of slug return and force sensor signals are captured in the process and classified by an expert and trained into an expert system for further prediction of the tool condition. Lee et. al. [22] purposed an adaptive time-series analysis and pattern recognition techniques to supervise punch wear by the blanking force signal. Ge et. al. [23] used a support vector machine based on strain sensors to predict fault processes. Klingenberg et. al. [16] presented a condition-based maintenance based on the force-displacement curve of the punch. The maximum force and displacement at that point are shown as promising features. Hernandez et. al.[5] proposed a new parameter, the effective clearance, to study wear. Also attempts with artificial neural network(ANN) are made. Shari et al. [24] showed monitoring the process by a vibration-based method. Hoppe

et. al. [7] showed a comparison of engineered features and feature extraction. Hambli [25] trained a neural network with a large number of FE Simulation to predict the height of the burr. Other ANN [26] model the blanking process and the related fine-blanking process [27] and its wear by back propagation neural networks. Kubik et. al. [28] correlated the force-displacement curve with varying process parameters. A feature-based correlation is used. Also, a guidance for detecting erroneous conditions is developed.

The ultimate goal is to determine when the punch needs to be replaced. This decision is often made based on experience without knowing the actual condition of the cutting tool/punch. In order to obtain a complete picture of tool condition, a disassembly of the entire cutting tool would be necessary, a cumbersome procedure [20]. A broken punch often causes major damage, costs and downtime. Therefore the punch is often replaced sooner rather than later. With this approach, however, it is never known how many components can still be produced. The optimal point in time to replace the punch would be when its lifetime has been reached or the degrading quality of the parts can no longer be tolerated. For optimal resource utilization and economy, the replacement point should be as close as possible to this optimal point. Instead of the punch itself, their condition can be estimated by sampling the condition of the cutting surface, which is more accessible. To our best knowledge the current state-of-the-art of inline measurement systems for quality monitoring of the stamping process is deduced by engineered features. However, these investigations are often verified by a small number of specimens. In terms of the large parameter space, a continuous quality measurement of the cutting surface is required.
The current methods of cutting surface analysis prevent a direct correlation between the influence of parameters and the quality of the parts. Current methods always require samples to be taken and analysed separately from the process. This is a crucial drawback for an industry which faces even shorter development processes with increased quality requirements as well as customized and application-individualized products. Therefore an economic process design using empirical knowledge or the trial-and-error method is not possible [29].

Cutting surface measurement

For the cutting surface analysis different measurement methods are used. Metallography micro section and contour gauges are the oldest, which suffer from the inaccuracy of the subjective reading of the values and from the tactile procedure. Behrens et al. [4] developed a device with a higher degree of automation for a measurement based on laser triangulation and a curve-matching-algorithm. Although the part must be prepared for the measurement the cutting surface parameters are detected automatically by the algorithm. For quality control of coils during manufacturing a chromatic confocal sensor is provided by Burghardt+Schmidt GmbH (Germany). Only the rollover, burr height and fracture angle can be measured. All these measuring methods only deliver partial or not reproducible results, require significant amount of time and only measure one profile section. This is a drawback because of the fluctuating cutting surface parameters over the surface. The transition from one cutting surface parameter to a another is not smooth and constant rather than depending on e.g., material variations. If a larger area of the surface has to be observed often a confocal microscope is used. While the high accuracy is an advantage, confocal microscopy is a time-consuming measurement because the surface has to be scanned several times; in addition, the microscope is a high price instrument. Further a survey with experts from different companies showed that there is no common standard for cutting surface analysis and documentation. Rather the metrics are defined with each customer separately. This leads to time consuming negotiations with every customer and to many different approaches for cutting surface analysis even within one company.

The goal of our contribution is twofold. First, we want to provide a monitoring system that is capable of measuring the shape and the texture of the cutting surface of produced parts, thus providing clear and reproducible metrics — including the variability along the surface — to derive and document the quality of the parts. This enables manufacturers to provide a 100 % quality inspection and customers to standardize the quality requirements. Second, an inline monitoring system for cutting surface properties provides the chance to link machine parameters to quality metrics, as described by [3]. As an example, we show that the punch condition is reflected in the burnish height over time, which can be used to determine the ideal point in time for predictive maintenance.

2 Optical monitoring system

Monitoring by an optical system seems to be particularly suitable for this task. Optical methods ensure high processing speeds and through combination with image processing a high degree of automation and reproducibility of measurement results. Furthermore, all optical measuring methods combine the properties of high accuracy and non-contact inspection. The developed system captures data of cutting surface parameters within the process for each part. It combines an image capturing and a triangulation method. Both share the same CMOS-sensor and a telecentric lens (see Figure 4). This expands the analysis into a surface view rather than only a (traditional) profile section of the cutting surface. For the development, a rectangular punch with dimensions

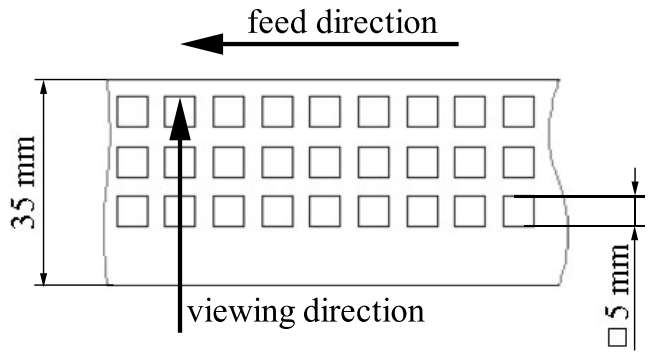

Fig. 3: Simplified produced stamping part which was used to design and test the developed monitoring system

$5 \times 5\,\mathrm{mm}^2$ and a coil material with a minimum thickness of 0.5mm was used (see Figure 3). With respect to the accuracy of the measured cutting surface parameters, we aim for an accuracy of $\pm 5\mu$m for all linear measures, which corresponds to $\pm 1\%$ of the coil thickness, and $\pm 1^\circ$ for the angular measure. For the production a Bihler GRM-NC was used with a maximum production speed of 250 strokes/minute. The system was placed close to the tool outlet.

2.1 Image capturing

The image capturing provides 2D images of the cutting surface and is used to determine most of the linear measures such as the burnish height. The required accuracy of the linear measures of $5\,\mu$m translates in an image resolution of $200\,\mathrm{linepairs/mm}$ at cutting surface level. To meet this requirement, we chose a telecentric lens with a magnification factor of $M = 2$ and a modulation transfer function (MTF) contrast of approximately 35 % at the desired image resolution. According to Nyquist sampling theorem the image sampling distance at sensor level needs to be $2.5\,\mu$m or less such that we decided for a sensor with a pixel pitch of $p = 4.8\,\mu$m. The closed contour of the stamping geometry does not allow a head-on setup. The optical axis of the lens can not be set orthogonal to the cutting surface. The whole system has to be tilted downward with respect to the horizontal plane (see Figure 4). This in turn leads to a perspective distortion of the 2D cutting surface image and hence leads to a reduction of achievable image resolution in vertical direction. With the given pixel pitch p one can calculate an upper limit $\gamma_{\max}$ for the tilt angle with $\arccos(p/5\,\mu\mathrm{m})$ resulting in an upper limit of $\gamma_{\max} = 16,3^\circ$. Due to space constraints, we chose for a slightly higher tilt angle of $\gamma = 20^\circ$ leading to a slightly lower resolution of approximately $195\,\mathrm{linepairs/mm}$ at cutting surface level. The tilting angle is ensured mechanically.

2.2 Triangulation

The triangulation method is capable to measure the 3D topography of the cutting surface and is used to determine the fracture angle β. Available laser triangulation sensors can not be used due to space constraints. Hence, we utilize the image capturing sensor for our triangulation by adding a laser line illumination. In this triangulation configuration (see Figure 4) the laser line illumination is orientated such that:

- the triangulation angle φ between the laser axis and the optical axis is set to $\varphi \approx 30^\circ$
- the laser line is orientated along the y_M-direction
- the laser line is imaged close to the center of the CMOS-sensor in x - direction

The sensor (2D)data of projected laser line across the cutting surface is transformed into the $x_\mathrm{M}, y_\mathrm{M}, z_\mathrm{M}$-coordinate system with the triangulation angle φ. The fracture angle β is extracted by projection this data the $y_\mathrm{M}, z_\mathrm{M}$-plane.

2.3 Components of the monitoring system

The monitoring system(see Figure 5a) consists of a telecentric lens with a magnitude $M = 2$ ($f = 75\,\mathrm{mm}, NA = 0.164$). An industrial camera (CMOS-sensor) with a pixel pitch of $p = 4.8\,\mu$m and a resolution of 1280 x 1024 Pixels (Field of view: 3.072 mm x 2.457 mm) and 170 fps and a laser module (Z-LASER Z30M18H3-F-450-lp45) with a wavelength of 470 nm which projects a line. The laser module comes with an adjustable focus ($f = 100\,\mathrm{mm}, 100\,\mathrm{kHz}$). All parts are mounted onto a baseplate. To adjust the laser line position in reference to the lens an adjustable mounting is received. This allows to rotate the laser in his own axis, adjust the triangulation angle and shift the laser position along the image x-axis. The illumination(see Figure 5b) is realized with two flashes (470 nm). It is crucial set up one flash above the part. The angle between the normal on the burnish surface and incoming light should be nearly the same as the angle between the normal and optical axis. This ensures that the burnish surface is brightly illuminated. Because of the different roughness of the fracture surface and the different angle this enables a distinction to be made. The second flash is set up in such a way that the reflected light of the lower side of the part is reflected into the lens. The laser and the flashes are powered with 24 V and the output is controlled with a potentiometer. Both devices are connected to the camera for process control. The desired workflow is show in Figure 6.

2.4 Calibration of the triangulation setup

In order to obtain precise 3D data, the triangulation angle φ must be calculated through calibration. For this end a

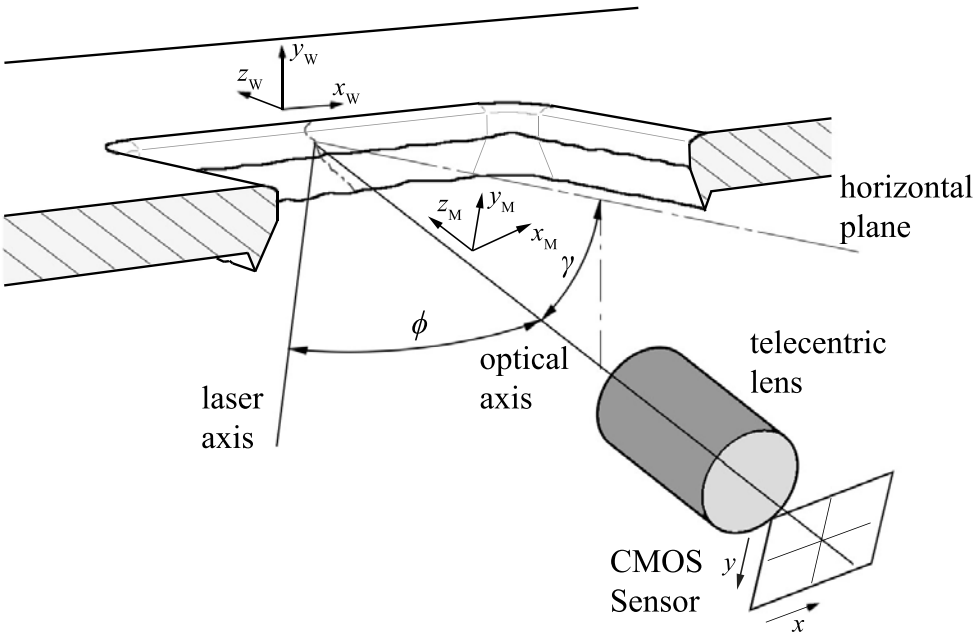

Fig. 4: Imaging and triangulation setup with tilt angle γ and triangulation angle φ

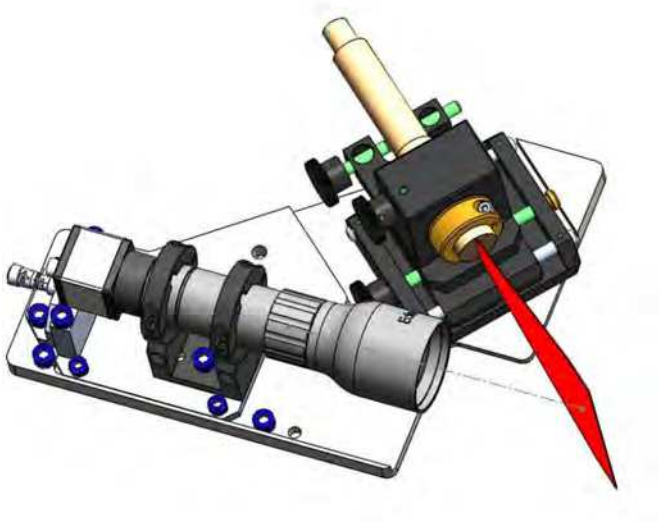

(a)

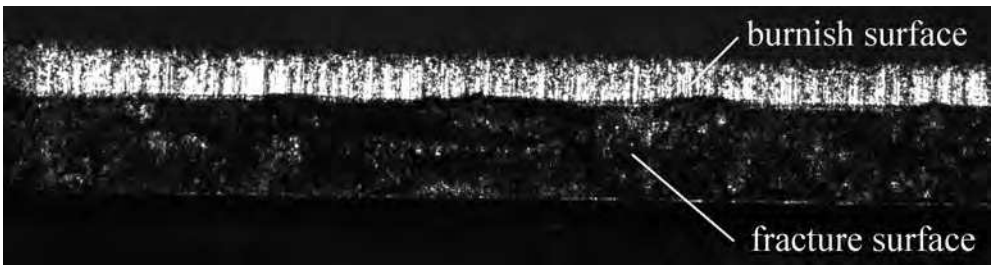

(b)

Fig. 5: (a) Optical monitoring system with sensor, lens, laser mounted onto the baseplate (b) image of a cutting surface

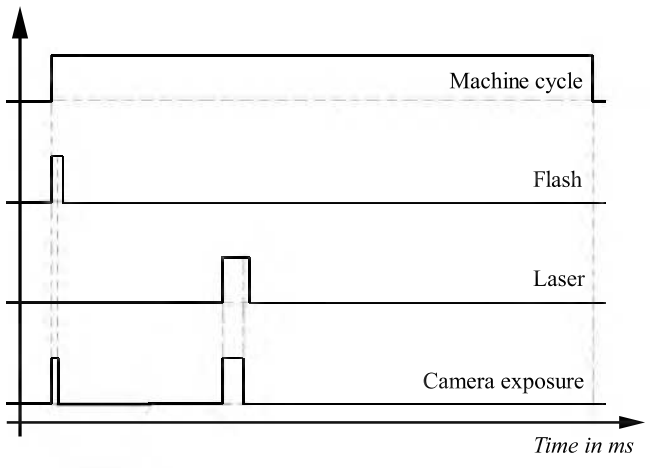

Fig. 6: Workflow of the monitoring system

calibration target with four different height levels is used (see Figure 7b). A confocal microscope (Keyence Corporation VK-X-100) was used to quantify the height levels z_c of the target in high precision. For the calibration procedure the monitoring system is placed in front of a motorized stage. The calibration target is mounted onto the stage(see Figure 7a). It is ensured that the optical axis of the imaging system and the surface normal of the calibration target coincide. The laser is aligned such, that the laser line projected on a flat surface illuminates a single pixel column on the CMOS-sensor, only. The laser was projected onto the target and captured with the CMOS-sensor. In this data the different height levels of the calibration target show up as four line segments. Each segment shifted to each other in x-direction (see Figure 7c). To calculate φ the differences in x-direction between have to be known. With a center of mass(COM) calculation the average x-positions for each line segment was determined. The differences Δx between the line segments were determined. With the known physical height level the triangulation angle φ is calculated.

2.5 Influence of the tilting angle γ

As stated above, the whole monitoring system has to be tilted around the x_W-axis by $\gamma = 20°$. As a side effect, the laser line illumination, which is set during the calibration process, is no longer orientated along the y_W-direction. Instead, the laser line is titled as well. On a flat cutting surface orientated parallel to the $x_\mathrm{W}, y_\mathrm{W}$-plane the laser line will be rotated around the z_W-axis by $\gamma = 20°$. This has to be kept in mind, in order to correctly calculate the fracture angle β of the measured triangulation data along the projected laser line.
After calibration, the monitoring system was mounted onto a Bihler Machine. Special care was taken to ensure that the optical monitoring system can be removed for the calibration process.

3 Extracting data for process monitoring

3.1 Image processing for image capturing

For image processing the OpenCV package for Python was used. This is beneficial to create prototype applications rapidly. The captured images showed a bright stripe which is identified as the burnish surface(see Figure 5b). Our desired task was a segmentation process which delivers the edges of the burnish surface. From that edges the burnish height was calculated. Edge detection operations such as Sobel filters were not applicable. Since a connected segmentation line along the transition between burnish and fracture surface could not be ensured due to the inhomogeneous gray values inside the burnish surface. Active Contour methods enable it to distinguish despite this fluctuation and create a connected transition line even with missing data points based on weighting factors.[30, 31]
Active Contours or Snakes denote an iterative energy minimization procedure, which deform a curve influenced by energy contributions such as conformity with the underlying image or local curvature of the curve [32]. The curve energy is divided into parts. The inner energy of the curve consists of a point spacing and a curvature term controlling the smoothness and elasticity, where less stretched and bent curves are favoured. The external energy depends on the image features itself. The curve is described by a finite amount n of points. The minimization problem is solved iteratively. In each iteration step curve energy is calculated. A minimization is made by a gradient descent method. All points are moved along the gradient of the energy and the energy is calculated and compared to its predecessor. The process is stopped after a certain amount of iteration steps or after the energy change is smaller than a convergence threshold. Details are given in [32].
To control the elasticity and smoothness of the curve the weights ζ, η can be set, respectively. Also, the number of points have to be considered as a trade-off between a good approximation of the curve and speed of segmentation.
In order to attract the curve towards the interface between burnish surface and fracture surface, a feature image is derived from the original image, and the external energy of the curve is calculated based on the feature image.

Feature Image Since working with gradient decent, the purpose of the feature image(see Figure 9a) is to create descending values towards the interface between burnish and fracture surface, with minima's at the unknown transition. It is constructed by first adding a background image to the original image. The background image values are increasing with the

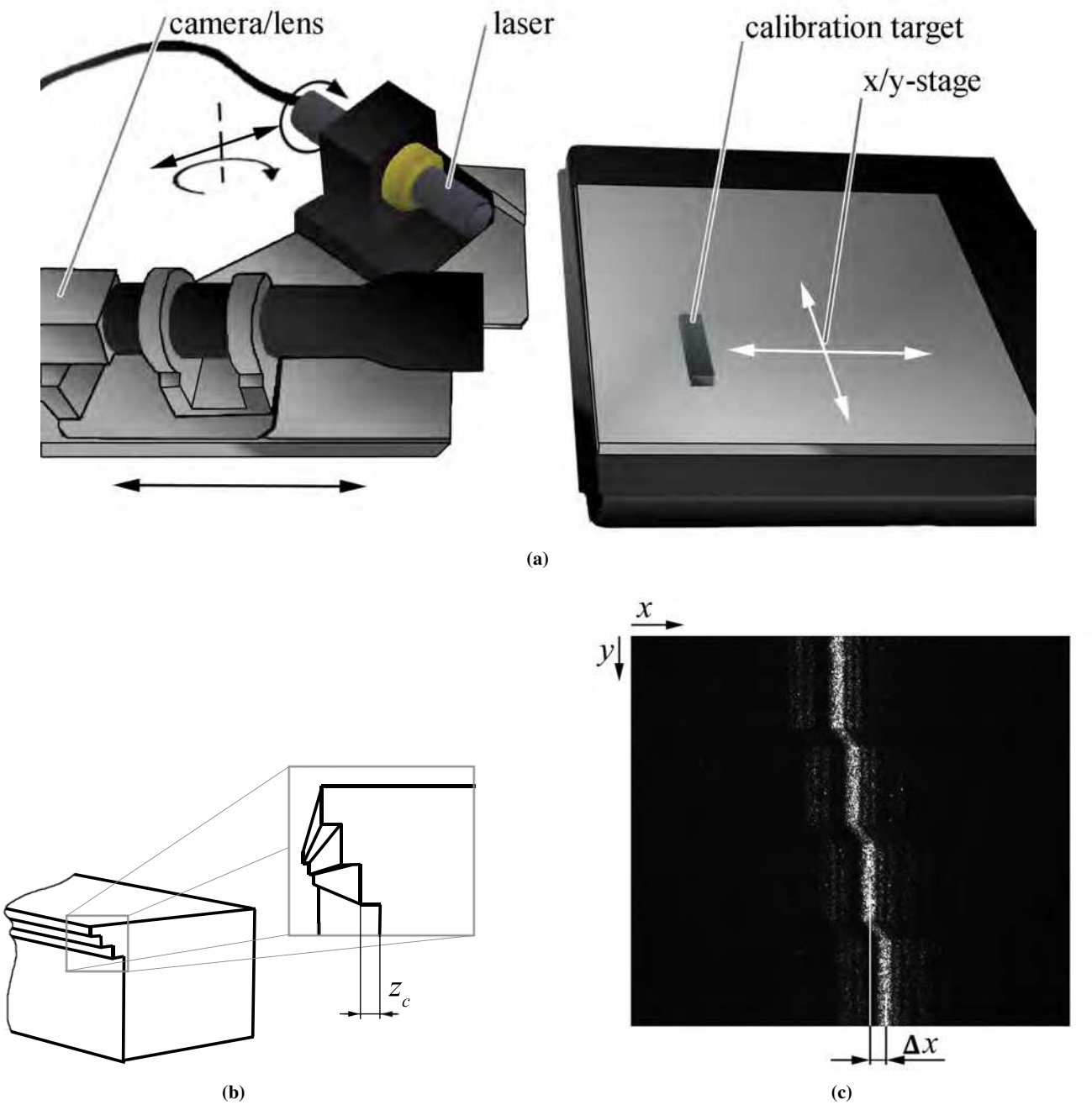

Fig. 7: (a) Calibration setup (arrows depict degrees of freedom) (b) Calibration target (c) Calibration Image

distance to the bright burnish surface. This new image can be seen as a 'ramp'(see Figure 9b,c) with decreasing structure towards the burnish surface. In addition, the gradient magnitude of the original image is subtracted from the new image. This decreases the intensity at the locations of the edges and ensures the minima to be at the transition.

Technically, the background image that ramps up towards the boundaries is found by a distance transform. We first determine the center of the burnish part by projecting the intensity along the x-axis and finding two y-coordinates such that all values with a projected intensity larger than 90% of the maximum intensity included between them (see Figure 8). The center coordinate is defined as the mean of those two y-coordinates. A distance transform then creates a ramp that is falling linearly towards the center of the burnish part. This image is called E_{ramp}. To add dependency to brightness the blurred Gaussian of the original image E_{Image} is added. The normalized gradient image E_{grad} which is obtain with a Sobel-Operation of the original image is subtracted. This is beneficial over the distance transform of the gradient be-

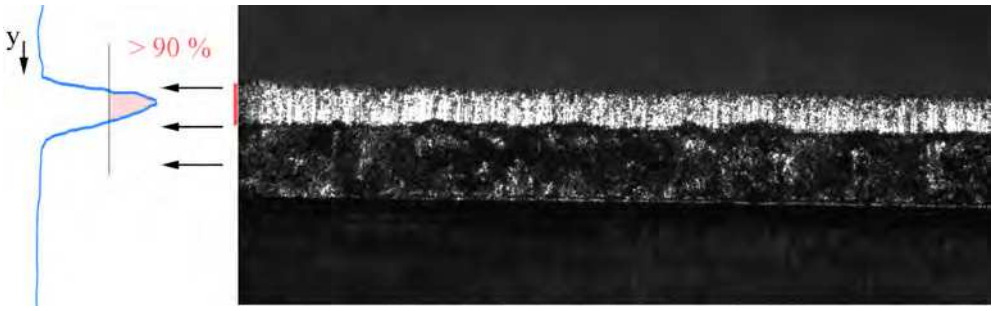

Fig. 8: Rough selection of the burnish part for creation of the feature image

cause this adds no offset. This results in the profile show in Figure 9b-c. The feature image concludes to:

$$E_{\text{ex}} = E_{\text{feat}} = \left[E_{\text{ramp}} + \kappa E_{\text{Image}} - \chi E_{\text{grad}} \right] \tag{2}$$

The factors κ, χ are for weighting the terms.

Initial Contour Since the burnish surface divides (see Figure 10) the image horizontally a closed contour is not required. It is a better approach to work with two open contours, one for the transition of the rollover/burnish surface and the other one for the transition of the burnish/fracture surface.
Active Contours are strongly dependent on the initial contour and the ratio of the weights $\zeta, \eta, \kappa, \chi$. To start with a contour which is close to the segmentation is beneficial in terms of processing time. Therefore an iterative process is carried out. A threshold value y_{height} has to be set by the operator. This serves as an estimate for the burnish height. At first the original image is divided along the x-axis into area segments of the same length. For each area a cumulative intensity projection within that length is performed. Again the y-coordinates with intensity level above a certain threshold are selected for each region. The maximum distance between these y-coordinates is calculated. With pixel pitch, magnification and tilting angle p, M, γ a compare value is calculated and compared to y_{height}. If the compare value is below y_{height} these boundary points are selected. If the compare value is greater than y_{height} the threshold is increased until condition one is satisfied. With the boundary points of all areas two curves are calculated. One for the upper and one for the lower contour.
Figure 11 shows the results of the image processing. The initial contour shown as blue lines and result of the segmentation shown as the red lines. The burnish height can be calculated with respect to pixel pitch, magnification and tilting angle p, M, γ.

3.2 Image processing for triangulation

The triangulation image (Figure 12a) shows the laser line projected onto the surface and viewed in the coordinate system of the CMOS-sensor. The triangulation image is mainly dark and only the laser line appears bright. The objective is to calculate the laser peak with sub pixel precision. Therefore, the laser image is blurred with a gaussian-kernel, and a region of interest (ROI) which only contains the data is defined by means of threshold. Background pixels are set to zero value. Since the laser diode sends a line with a certain thickness a center of mass algorithm can be performed (see Figure 12b). A fast-performing algorithm is desired. Therefore, only a 5-point neighbourhood around the maximum is used to compute the position of the peak $x_{\hat{\delta}}$ for every row $y_{\hat{\delta}}$. Details given in [33].
The estimated peak position $x_{\hat{\delta}}$, $y_{\hat{\delta}}$ are projected into the distance space with:

$$x_w = x_{\hat{\delta}} \cdot \sin(\gamma) \cdot \frac{p \cdot \tan\varphi}{M} + r \tag{3}$$

$$y_w = y_{\hat{\delta}} \cdot \sin(\gamma) \cdot \frac{\cos\varphi}{\sin\varphi} \tag{4}$$

$$z_w = x_{\hat{\delta}} \cdot \sin(\gamma) \cdot \frac{p \cdot \cos\varphi}{\sin\varphi \cdot M} \tag{5}$$

where x_w, y_w, z_w are the world-coordinates of the scanned surface points and r the travel distance between images. Multiple images combine to a scan of the cutting surface where the fracture angle β can be measured.

4 Verification and validation of the monitoring system

In order to validate the monitoring system several tests have been carried out. For the test of the 2D image processing images were recorded within the machine cycle and processed. The test for the triangulation data took place offline on the motorized stage. A confocal microscope was used for ground truth data acquisition

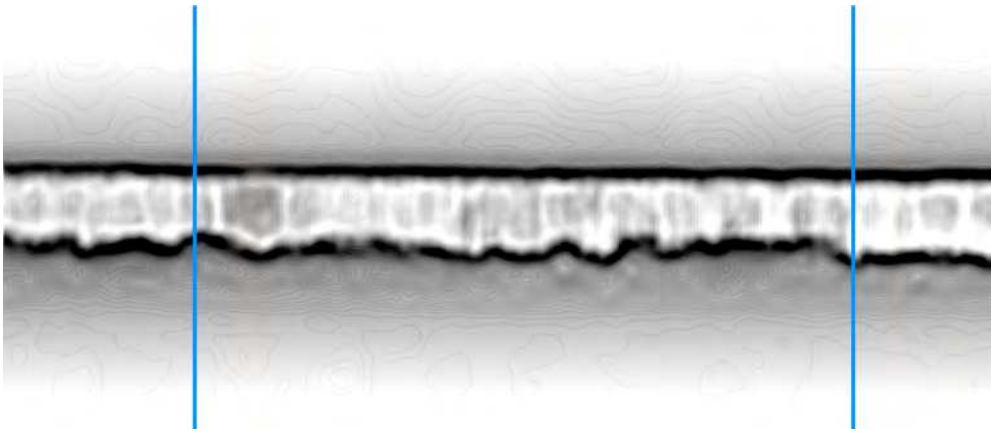

(a)

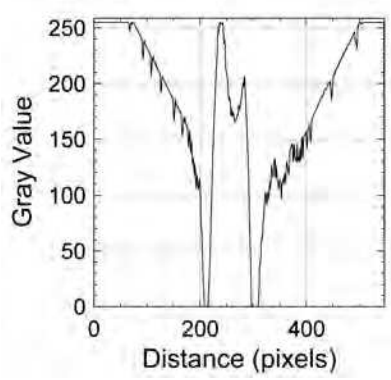

(b)

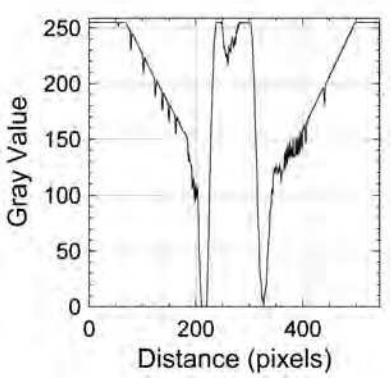

(c)

Fig. 9: (a) Feature Image (b) Profile of the left vertical line (c) Profile of the right vertical line

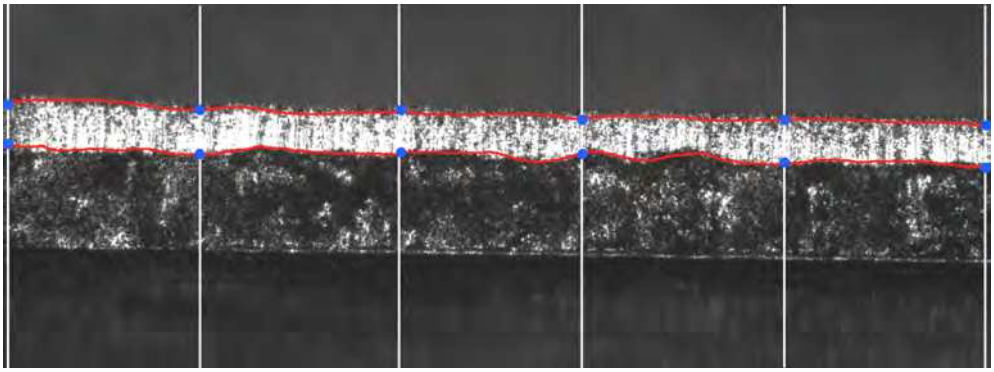

Fig. 10: Segments for initial contour. Each segment performs a cumulative projection of the intensity along their length. The distance of the y-coordinates which are below y_{height} are picked and represented as the blue points. The red curves are calculated based on these points.

Table 1: Transition settings

Transition	ζ	η	κ	χ
rollover/burnish	0.15	0.8	1.5	1.0
burnish/fracture	0.01	0.18	1.5	1.0

4.1 Validation of image processing

Three parts of stainless steel and copper each where manufactured and captured with the system (see Figure 11). These parts were taken from the production process and measured with a confocal microscope. Because of lack of definition of the cutting surface parameters in the surface view there is no clear feature for comparison. Although existing human heuristics a manual point-by-point comparison — between the microscope- and image processing-data — of the burnish heights is considered as a good approximation for the ground truth.
For each part three positions were tested. Here, particularly prominent places such as increases or decreases in the transition between burnish/fracture surface were selected. The settings for the image processing can be seen in Table 1. The initial contours were calculated from 20 image segments. The maximum allowed iterations set to 80 and the convergence limit was 0.0001.
The results of the validation can be seen in Table 2. The data shows good precision with a spread from + 4.28 to -2.70 % and mean of -0.68 %. This is within the desired accuracy of $\pm 5\,\mu$m. With the implementation in Python the processing of the images took 40 to 60 seconds. This implementation is not optimized for performance. Real time performance can be achieved with optimization and parallelization of the code.

4.2 Validation of triangulation data

To verify the triangulation method three cutting surfaces were recorded on the motorized stage. One scan consisted of 200 images with a step width in the x-axis of $r = 5\,\mu$m between them. For a clear assessment of the characteristics of the cutting surfaces and to scan the right area notches were made. The notched surfaces were also measured with the microscope and the measured surface was exported. The images of the triangulation were processed, and a point-cloud was calculated. The processing of all 200 images took about 20 seconds.
For the comparison of the data the surface from the microscope and the point-cloud were imported in the software CloudCompare. At first a manual alignment by picking point pairs was performed. Afterwards an automatic registration with the iterative closest point algorithm followed and the distance between surface and cloud was calculated. The same task was calculated with the free version of GOM Inspect for a cross check. Since there were many converting steps involved, differences can result from this. This can therefore only be seen as a qualitative verification.
The results of the three parts can be seen in Table 3. The visual output of the software for the surface to cloud distance can be seen in Figures 16, 17, 18. Both software products provided comparable results. The mean difference of the data generated by the image processing was always beneath $2\,\mu$m and their standard deviation was $10\,\mu$m. The notches were clearly visible in all data. The largest deviations are found at the strongly deformed burrs and the sharp surface changes in the area of the notches. They cause changes in reflection behaviour and thus create strong singularities. The microscope automatically corrects these behaviours whereas the sensor lacks this option. Therefore, these deviations can be neglected. Additionally, some geometries could not be scanned because they were occulted due to the triangulation angle. Therefore, delivered false or no data is also neglected. The results show that the desired accuracy of $\pm 5\,\mu$m was not achieved but the similar result show high confidence in the data.

5 Case study: capabilities in production

The capabilities of this monitoring system can be seen with an interesting example. We captured 17.000 images during a material test where punch failure occurred. This is novel because it is the first continuous data of the cutting surface within a process. We analysed the cutting edge of the used punch with the confocal microscope for wear within given intervals (5.000, 10.000, 25.000 strokes). Figure 13 shows the condition of the punch recorded with the microscope. A fully functional cutting edge at 5.000 and 10.000 strokes was observed. Whereas the cutting edge at 25.000 strokes was damaged. Within an interval of 15.000 strokes the point of failure can not be specified more closely. After the test has been carried out the captured images were processed for their burnish heights. The orientation of the punch in the cutting tool and the position of the failure is known. This position can be transferred to the image and appears on its left-end side. Figure 14 shows a selection of images from the monitoring system with the area of failure marked. Since there are images for every cutting surface the point of failure can be localized more precisely by manually analysing them. The failure emerged around the 13.500 strokes.
To gather additional information about the evolution of the failure the burnish height of two regions of each image have been compared. These regions were the known failure region(left-end of the image) and a fully functional region (right-end of the image). To consider the feed tolerance of the production machine of ± 0.1 mm the burnish heights were averaged over a range of 0.2 mm in the x-direction. The result for the analysed cutting surface in the interval from 7.000

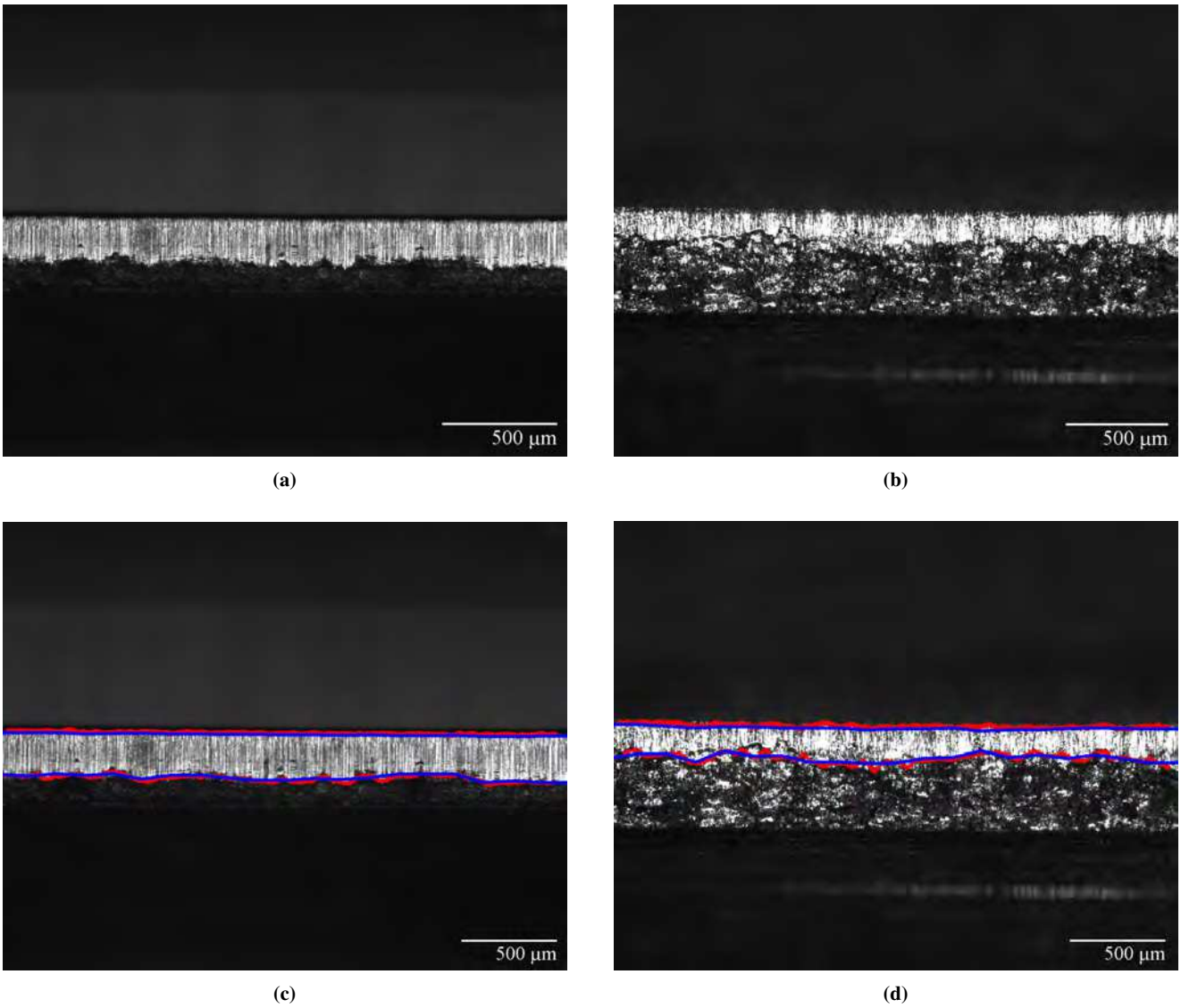

Fig. 11: (a) image of stainless steel (b) image of copper (c) segmentation of image a (d) segmentation of image blue line = initial contour, red line = segmentation

to 25.000 strokes can be seen in Figure 15. Even though the cutting edge of the punch was considered fully functional at 10.000 strokes with the confocal microscope one can see that burnish heights begin to decline from the start. The burnish height on the left-end shows a rapid decrease and higher fluctuation whereas the burnish height on the right-end stays on a constant level, despite the fluctuation caused by material- and process tolerances. Based on that data the evolution of the failure starts around 7.000 strokes. In comparison, the new system enables earlier detection of failure. The point of failure is also met around 13.500 strokes. The following reapproach (grey) to the right-end graph is misleading. The produced surface quality of a worn-out punch still creates portions of burnish surface which are detected by the algorithm. These portions are often shifted to the normal burnish part or not continuous and thereby do not meet the quality requirements or the definition of the cutting surface parameters on which the developed algorithm is based. In the sense of predictive maintenance this result can be used for better planning reliability and following processes. A faster image processing would enable to view the graph during production.

6 Conclusion

Measuring meaningful metrics of the cutting surface of stamping parts is key for process optimization and quality management but is still not implemented in real time in commercial stamping machines. We developed a combined 2D/3D optical

Table 2: Comparison of the burnish height between the monitoring system and the microscope

	Optical Unit in μm	Microscope in μm	Spread in %
stainless steel 1	151.678	155.890	2.70
	133.234	130.545	-2.06
	138.097	139.541	1.03
stainless steel 2	138.852	133.148	-4.28
	133.560	134.507	0.70
	154.533	151.391	-2.08
stainless steel 3	136.259	134.156	-1.57
	161.619	160.030	-0.99
	135.242	131.534	-2.82
copper 1	194.982	193.002	-1.03
	205.210	203.003	-1.09
	176.508	175.883	-0.35
copper 2	170.842	170.067	-0.46
	173.656	174.101	0.26
	171.291	173.201	1.10
copper 3	175.270	173.260	-1.16
	146.591	144,894	-1.17
	189.461	192.739	1.70
Mean			-0.64

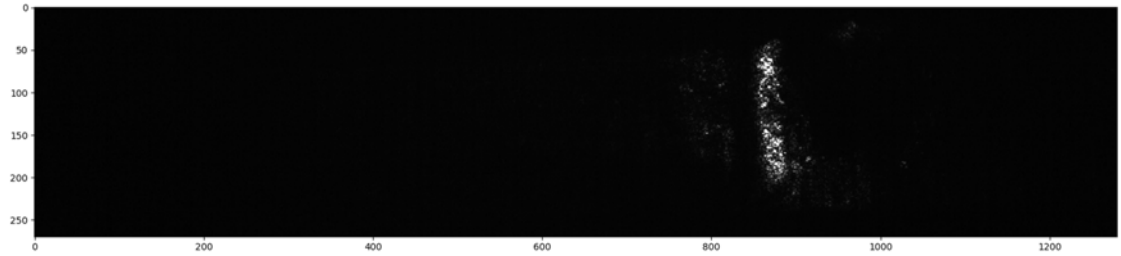

(a)

(b)

Fig. 12: (a) triangulation image (b) segmentation of the triangulation image

Table 3: Deviation between reference surface and measured point-cloud in *mm*

	Part 1	Part 2	Part 3
mean(CloudCompare)	0.002	0.001	0.0002
mean(GOM Inspect)	0.0019	0.004	0.0002
Standard deviation(CloudCompare)	0.0092	0.0050	0.0153
Standard deviation(GOM Inspect)	0.0094	0.0031	0.0129

monitoring system with corresponding image processing of stamping parts and integrated it into a commercial stamping machine. Unlike state-of-the-art methods that rely on the extraction of parts, this system captures data from the cutting surface within the process cycle. The image processing allows for an automatic and accurate measurement of 2D and 3D parameters of the cutting surface for every stroke. It is now possible to monitor the quality of produced parts over the tool lifetime. Moreover, displaying key characteristics of the cutting surface in (near) real time supports the worker

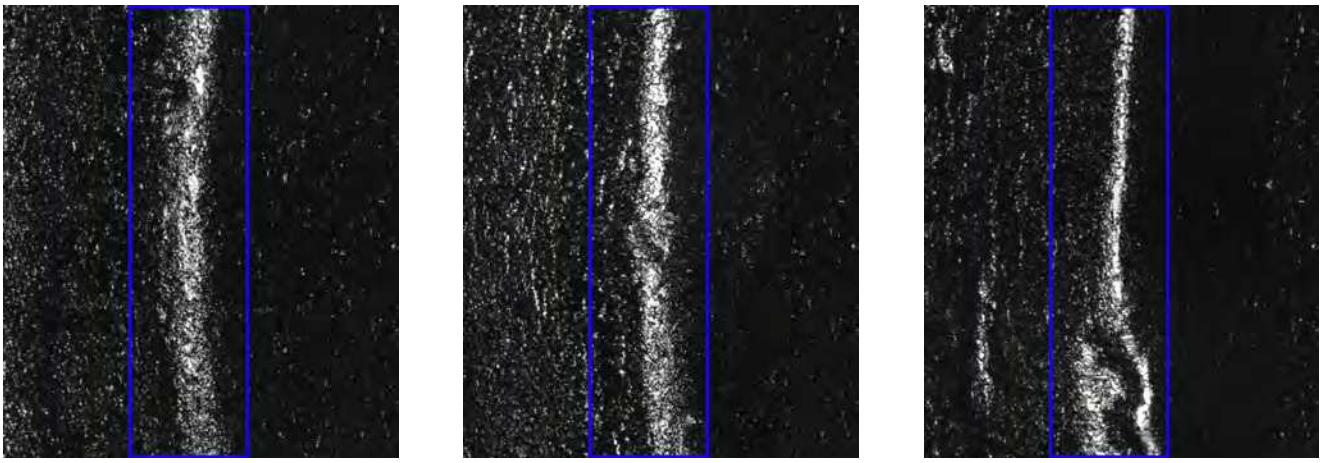

(a) (b) (c)

Fig. 13: Confocal microscope images of the cutting edge (highlighted blue box) of the punch (a) cutting edge (punch) 5.000 strokes (b) cutting edge (punch) 10.000 strokes (c) worn out cutting edge (punch) 25.000 strokes

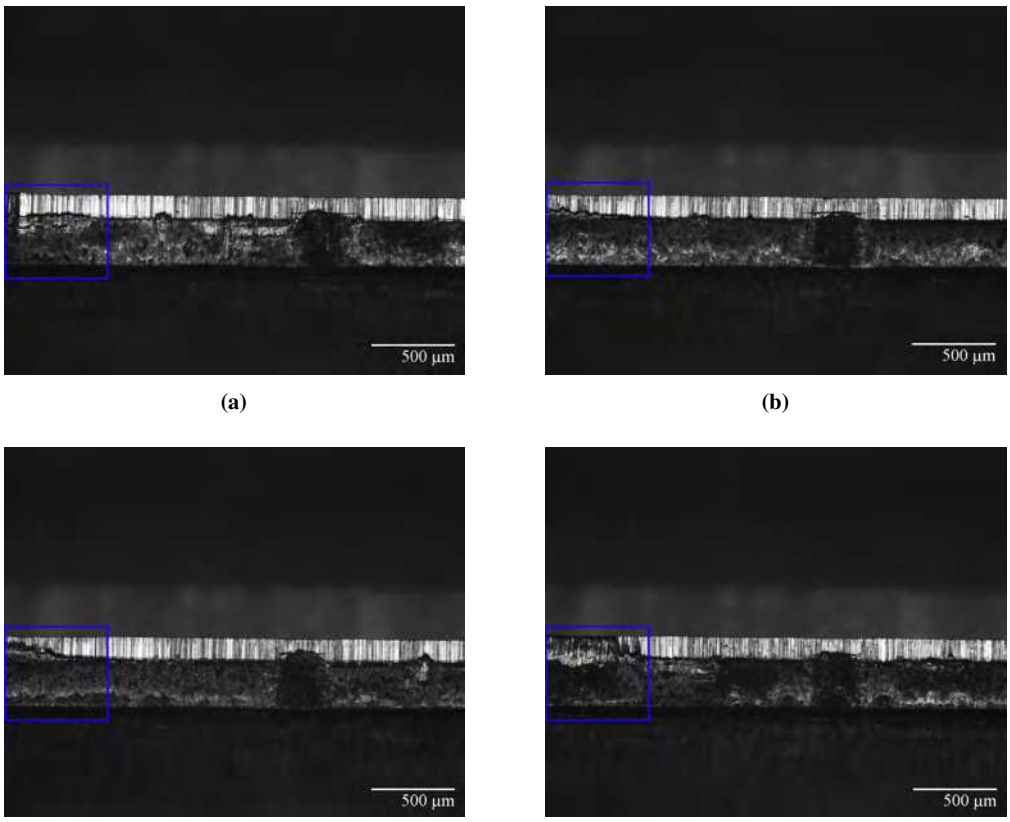

(a) (b)

(c) (d)

Fig. 14: (a) cutting surface 10.000 strokes (b) cutting surface 13.000 Strokes (c) cutting surface 13.500 strokes (d) cutting surface 25.000 strokes

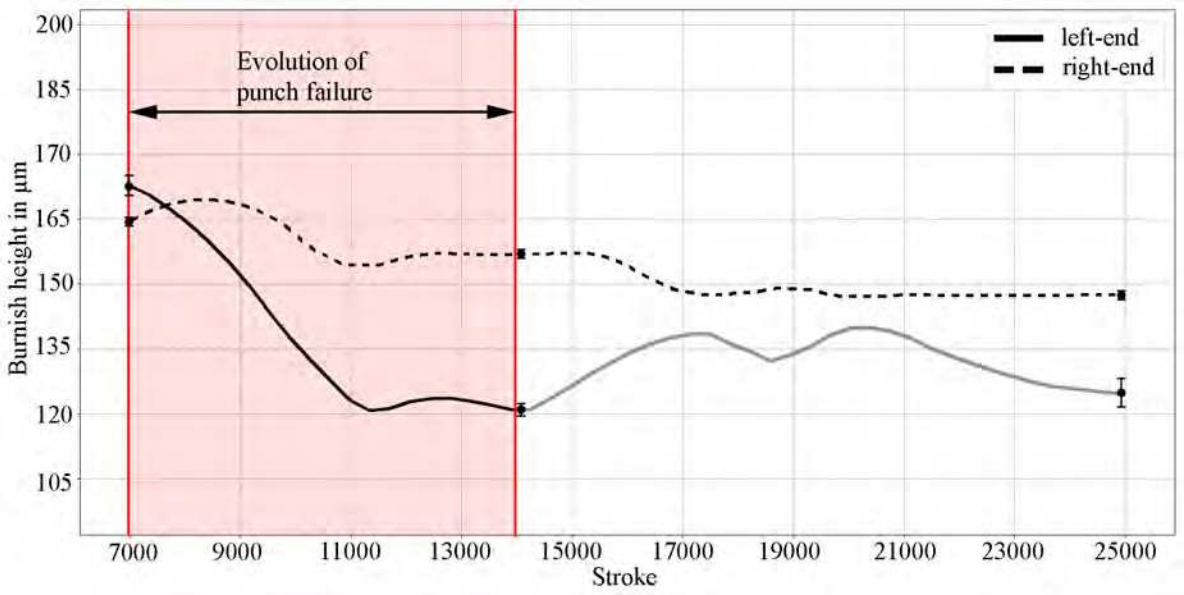

Fig. 15: Diagram of the burnish height at the left- and right-end of the Image

during the production. Within a case study we provide first data that show how such a system can be used in the context of predictive maintenance. Our case study focuses on the evaluation of the burnish height with data that was collected within the process cycle. We verified the image processing for the 2D and 3D parameters with ground truth data. Although only evaluated offline at the moment, in theory it is possible for the image processing to be accomplished within the process cycle time.

Future research will focus on the collection of production triangulation data and image processing within the process-cycle. Variations of the stamping process will be analysed on a stroke-to-stroke basis. This can lead to new insights into the process and the definition of new quality metrics. In terms of predictive maintenance, the increase and decrease of the cutting surface parameters over the lifetime of the punches will be investigated. With more data a correlation between process parameters and quality of the product and wear could be established. This could lead to a lifetime prediction of the punch/tool. Furthermore, this monitoring system is an important step towards data driven modelling of the stamping process. An accurate model relies heavily on the process output, which can now captured for the first time with our system. In combination with a multi sensor network this could finally lead to an increased process understanding and a highly efficient, self-regulating stamping process.

Funding The Authors gratefully acknowledge financial support from the interdisciplinary technology network Efficient Production Technology (EffPro), co-funded by the European Union and the Free State of Bavaria from the European Fund for regional development (ERDF) and supported by the University of Applied Sciences Kempten and the Bavarian Ministry of Science and Art.

Availability of data and material The data that support the findings of this study are available from the corresponding author on reasonable request.

Code availability For Image processing a custom code was implemented in Python. The Software GOM Inspect(Freeware) and CouldCompare(GNU) were used for 3D-Data comparison.

Declarations

Conflicts of interest The authors declare that they have no conflict of interest.

References

1. Schomaker KH (1994) Prozessüberwachung und Diagnoe mit optoelektronischen Messeinrichtungen an Schneidpressen. VDI Verlag GmbH, Hannover
2. Kim JD, Kim HK, Heo YM, Chang SH (2012) A study on die roll height of special automobile seat recliner gear according to die chamfer shape in fine blanking tool. Applied Mechanics and Materials 121-126:3694–3699, DOI 10.4028/www.scientific.net/AMM.121-126.3694
3. Hoogen M (1999) Einfluß der Werkzeuggeometrie auf das Scherschneiden und Reißen von Aluminiumfeinblechen: Zugl.: München, Univ., Diss., 1999, utg-Forschungsberichte, vol Bd. 6. Hieronymus, München
4. Behrens BA, Jocker J (2013) Optische Schnittkantenmessung und automatisierte Kenngrößenermittlung: Ergebnisse eines Vorhabens der Industriellen Gemeinschaftsforschung (IGF), EFB-Forschungsbericht, vol Nr. 385. EFB, Hannover
5. Hernández JJ, Franco P, Estrems M, Faura F (2006) Modelling and experimental analysis of the effects of tool wear on form errors in stainless steel blanking. Journal of Materials Processing Technology 180(1-3):143–150, DOI 10.1016/j.jmatprotec.2006.05.015
6. Verein Deutscher Ingenieure (1994) Schnittflächenqualität beim Schneiden, Beschneiden und Lochen von Werkstücken aus Metall Scherschneiden: VDI2906
7. Hoppe F, Hohmann J, Knoll M, Kubik C, Groche P (2019) Feature-based supervision of shear cutting processes on the basis of force measurements: Evaluation of feature engineering and feature extraction. Procedia Manufacturing 34:847–856, DOI 10.1016/j.promfg.2019.06.164
8. Krinninger M, Opritescu D, Golle R, Volk W (2017) On the opportunities of problem- and process-adapted shear cutting simulations for effective process design. Procedia Engineering 207:1570–1575, DOI 10.1016/j.proeng.2017.10.1080
9. Feistle M, Krinninger M, Paetzold I, Stahl J, Golle R, Volk W (2017) Design and conceptualization of a cutting tool to investigate the influence of the shear cutting process on edge crack sensitivity. Journal of Physics: Conference Series 896(1), DOI 10.1088/1742-6596/896/1/012106
10. Lange K (1990) Umformtechnik: Handbuch für Industrie und Wissenschaft, zweite, vö edn. Springer Berlin Heidelberg, Berlin, Heidelberg and s.l., DOI 10.1007/978-3-662-10686-0
11. Klocke F, König W (2006) Fertigungsverfahren 4: Umformen, 5th edn. VDI-Buch, Springer-Verlag Berlin Heidelberg, Berlin, Heidelberg, DOI 10.1007/978-3-540-39533-1
12. Cheon S, Kim N (2016) Prediction of tool wear in the blanking process using updated geometry. Wear 352-353:160–170, DOI 10.1016/j.wear.2016.01.024
13. Hambli R (2003) BLANKSOFT: A code for sheet metal blanking processes optimization. Journal of Materials Processing Technology 141:234–242, DOI 10.1016/S0924-0136(03)00161-4
14. Hambli R (2002) Design of experiment based analysis for sheet metal blanking processes optimisation. International Journal of Advanced Manufacturing Technology 19(6):403–410, DOI 10.1007/s001700200041
15. Slomp J, Klingenberg W (2004) A Proposal to Use Artificial Neural Networks for Process Control of Punching / Blanking Operations. Flexible Automation and Inteligent Manufacturing pp 556–562
16. Klingenberg W, de Boer TW (2008) Condition-based maintenance in punching/blanking of sheet metal. International Journal of Machine Tools and Manufacture 48(5):589–598, DOI 10.1016/j.ijmachtools.2007.08.013
17. Breitling J, Pfeiffer B, Altan T, Siegert K (1997) Process control in blanking. Journal of Materials Processing Technology 0136(97)
18. Hohmann J, Schatz T, Groche P (2017) Intelligent Wear Identification Based on Sensory Inline Information for a Stamping Process
19. Wadi I, Balendra R (1999) Using neural networks to model the blanking process. Journal of Materials Processing Technology 91(1):52–65, DOI 10.1016/S0924-0136(98)00426-9
20. Monteil G, Gréban F, Roizard X (2008) In situ punch wear measurement in a blanking tool, by means of thin layer activation. Wear 265(5-6):626–633, DOI 10.1016/j.wear.2007.12.014
21. Mardapittas AS, Au, Y, H J (1992) BETS: An Expert Syastem for Tool condition Monitoring in Blanking. In: Shirvani B, Baggs DRH (eds) Proceedings of the International Conference of Sheet Metal, IOP Publishing, London, pp 141 – 150
22. Lee WB, Cheung CF, Chiu WM, Chan LK (1997) Automatic supervision of blanking tool wear using pattern recognition analysis. International Journal of Machine Tools and Manufacture 37(8):1079–1095, DOI 10.1016/S0890-6955(97)88104-7
23. Ge M, Du R, Zhang G, Xu Y (2004) Fault diagnosis using support vector machine with an application in sheet metal stamping operations. Mechanical Systems and Signal Processing 18(1):143–159, DOI 10.1016/S0888-3270(03)00071-2
24. Sari D, Wu TL, Lin BT (2016) Preliminary study for online monitoring during the punching process. International Journal of Advanced Manufacturing Technology 88:2275–2285, DOI 10.1007/s00170-016-8956-y

25. Hambli R (2002) Prediction of burr height formation in blanking processes using neural network. International Journal of Mechanical Sciences 44(10):2089–2102, DOI 10.1016/S0020-7403(02)00168-6
26. Al-Momani ES, Mayyas AT, Rawabdeh I, Alqudah R (2011) Modeling Blanking Process Using Multiple Regression Analysis and Artificial Neural Networks. Journal of Materials Engineering and Performance 21(8):1611–1619, DOI 10.1007/s11665-011-0079-x
27. Yin F, Mao H, Hua L, Gu Z (2012) Back propagation neural network based calculation model for predicting wear of fine-blanking die during its whole lifetime. Computational Materials Science 59:140–151, DOI 10.1016/j.commatsci.2012.03.008
28. Kubik C (2021) Exploitation of force displacement curves in blanking — feature engineering beyond defect detection blanking process b) partition the cutting edge surface h e rollover zone h l shear zone h f rupture zone pp 261–278
29. Bauernhansl T, ten Hompel M, Vogel-Heuser B (2014) Industire 4.0 in Produktion, Automatisierung und Logistik p 648
30. Chan TF, Vese LA (2001) Active contours without edges. IEEE Transactions on Image Processing 10(2):266–277, DOI 10.1109/83.902291
31. Ngan KN, Meier T, Chai D (1999) Chapter 4 - Model-Based Coding. In: Ngan KN, Meier T, Chai D (eds) Advanced Video Coding: Principles and Techniques, Advances in Image Communication, vol 7, Elsevier, pp 183–249, DOI https://doi.org/10.1016/S0928-1479(99)80006-0
32. Kass M, Witkin A, Terzopoulo D (1988) Snakes: Active Contour Models. International Journal of Computer Vision 1:321–331, DOI https://doi.org/10.1007/BF00133570
33. Fisher R, Naidu D (2001) A Comparison of Algorithms for Subpixel Peak Detection. Image Technology, Advances in Image Processing, Multimedia and Machine Vision DOI 10.1007/978-3-642-58288-2-15

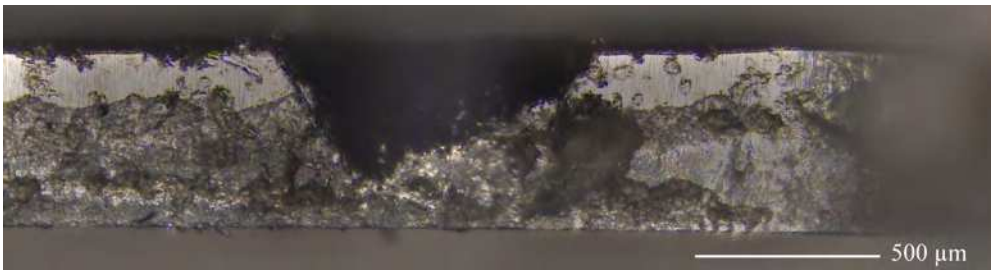

(a)

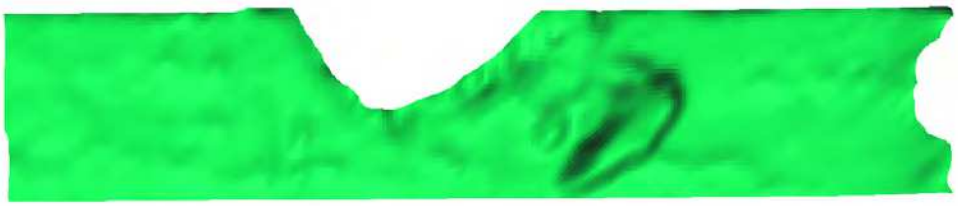

(b)

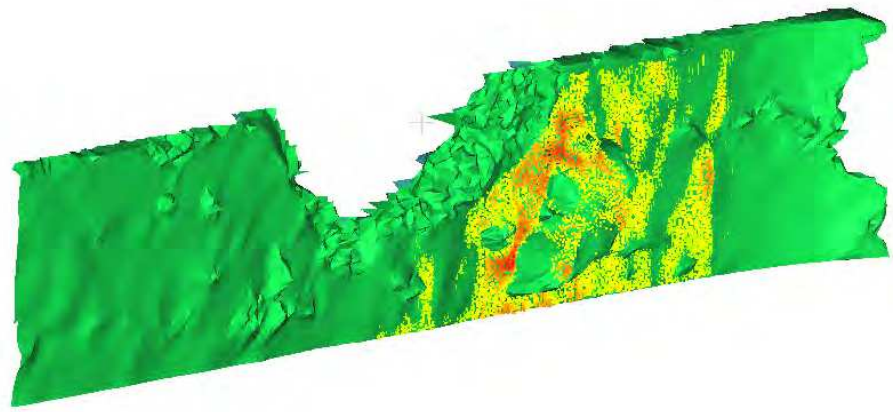

(c)

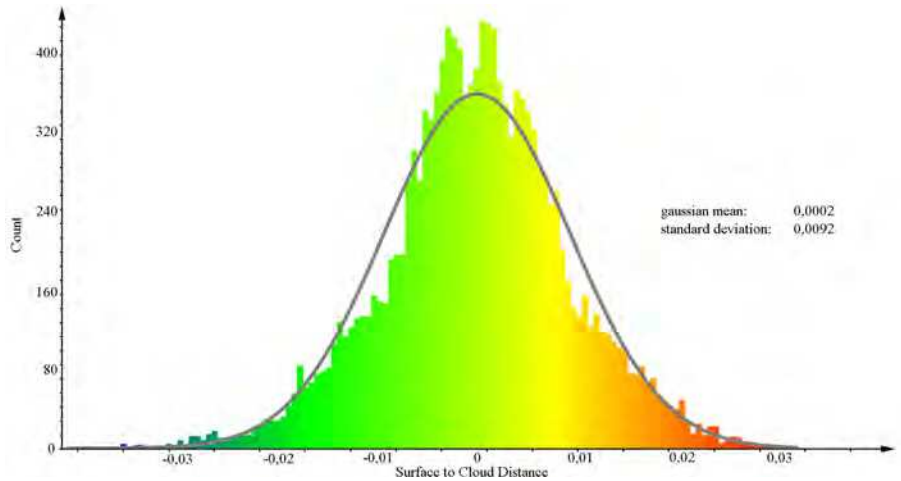

(d)

Fig. 16: Part 1 (a) microscope image (b) surface from microscope (c) surface to cloud distance with aligned cloud (d) histogram of surface to cloud distance distribution

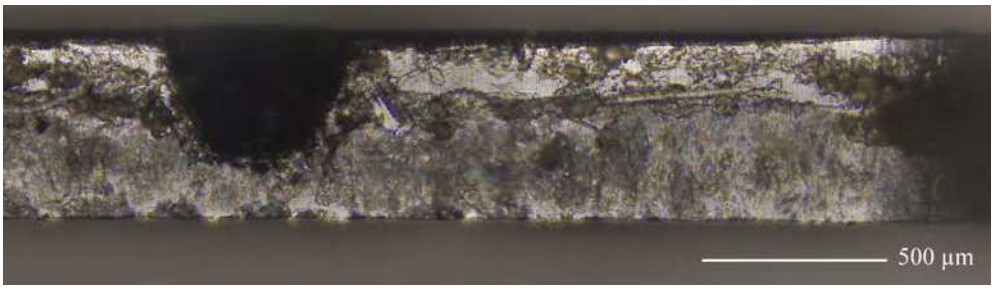

(a)

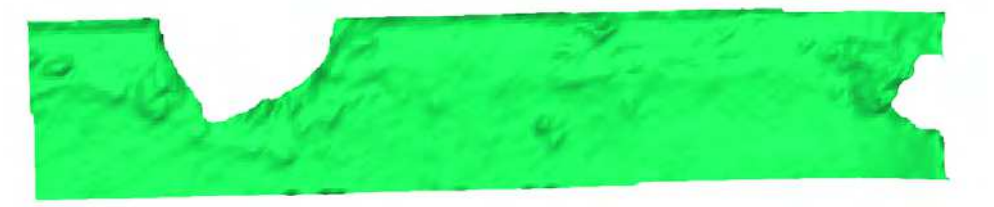

(b)

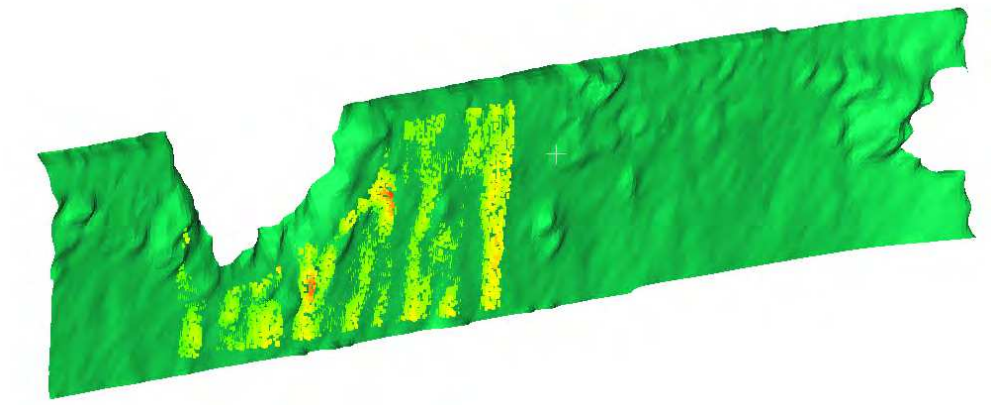

(c)

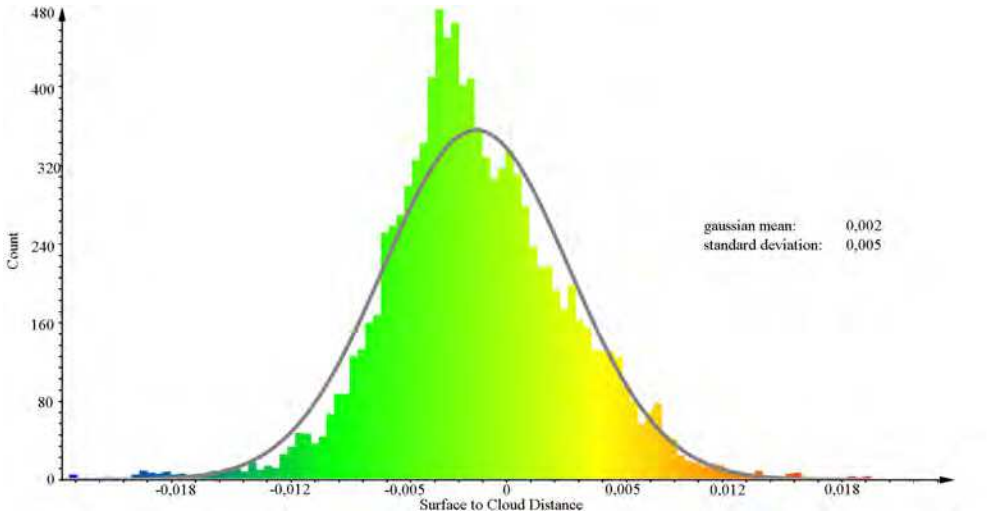

(d)

Fig. 17: Part 2 (a) microscope image (b) surface from microscope (c) surface to cloud distance with aligned cloud (d) histogram of surface to cloud distance distribution

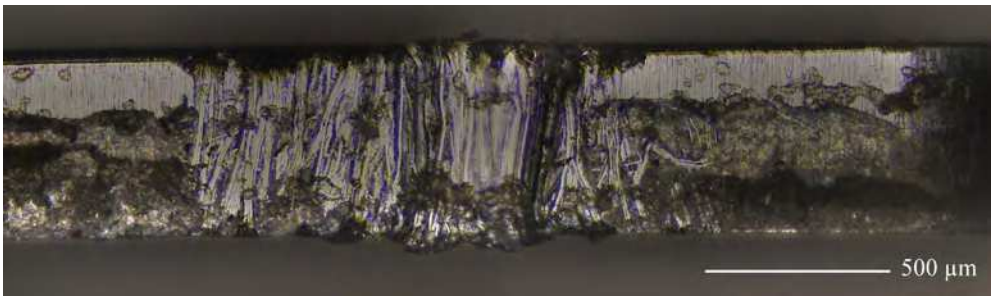

(a)

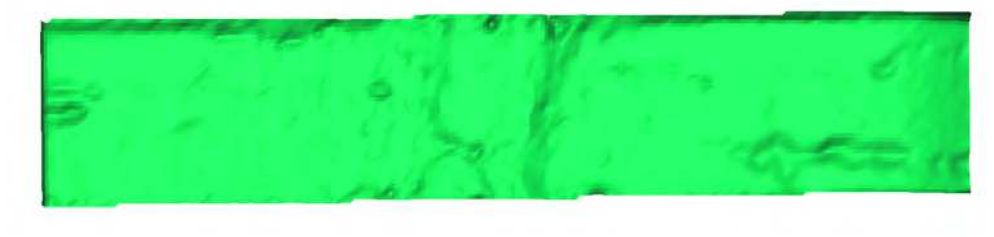

(b)

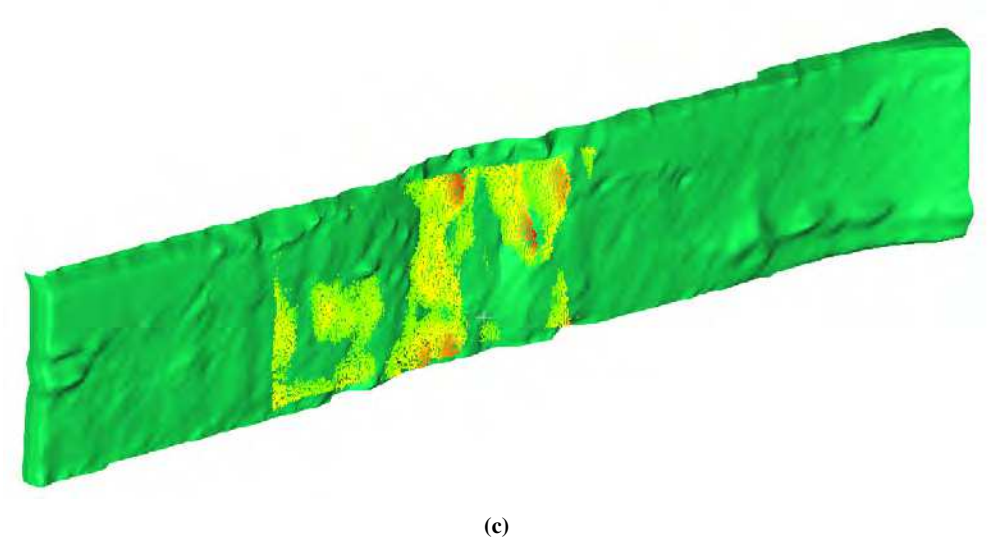

(c)

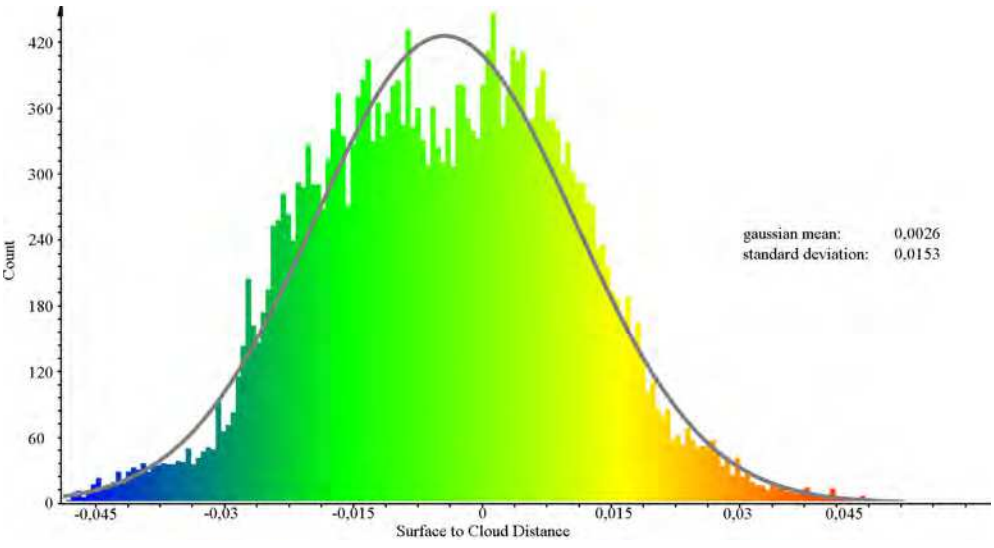

(d)

Fig. 18: Part 3 (a) microscope image (b) surface from microscope (c) surface to cloud distance with aligned cloud (d) histogram of surface to cloud distance distribution

Figures

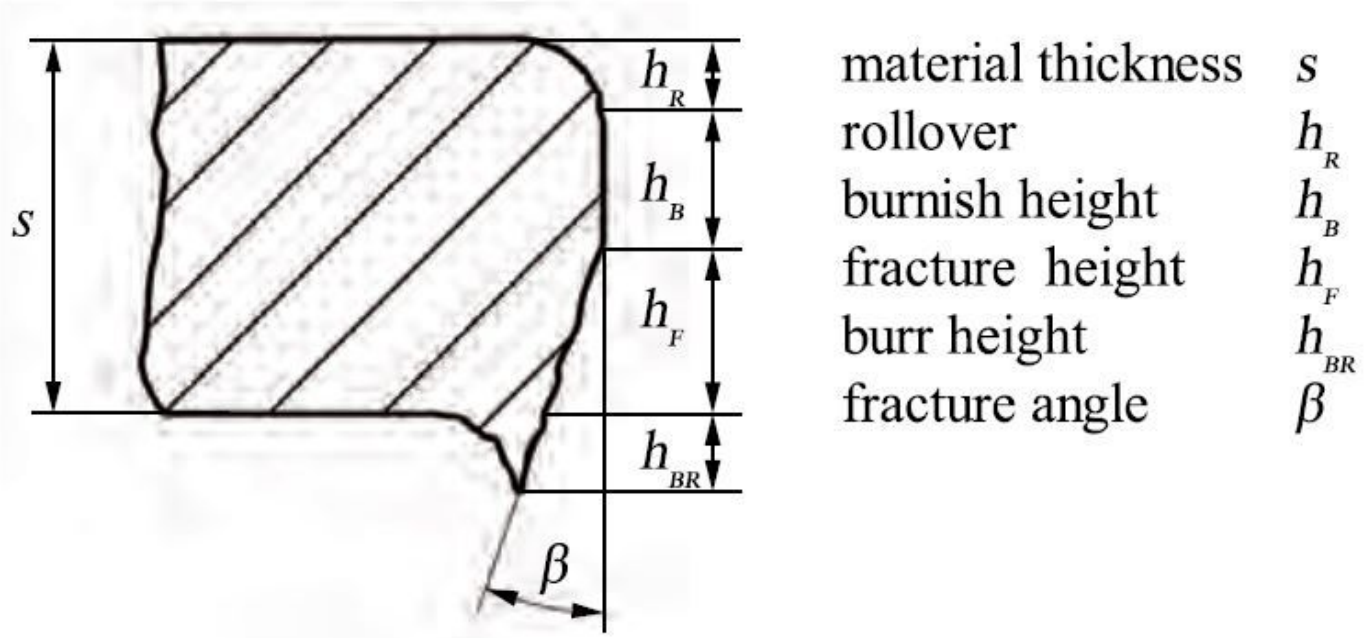

Figure 1

Definition of the cutting surface parameters [6]

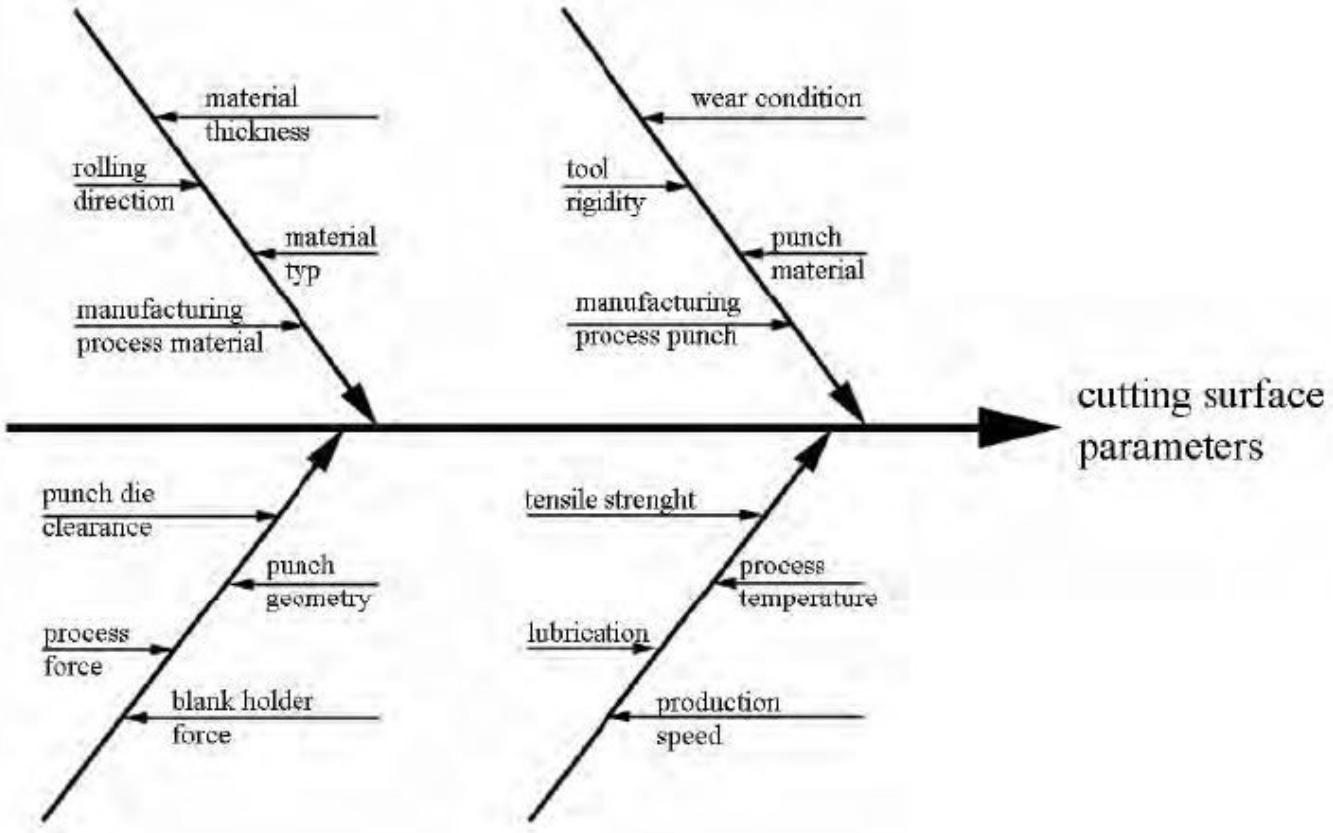

Figure 2

Selection of process parameters that are most likely to influence the cutting surface parameters

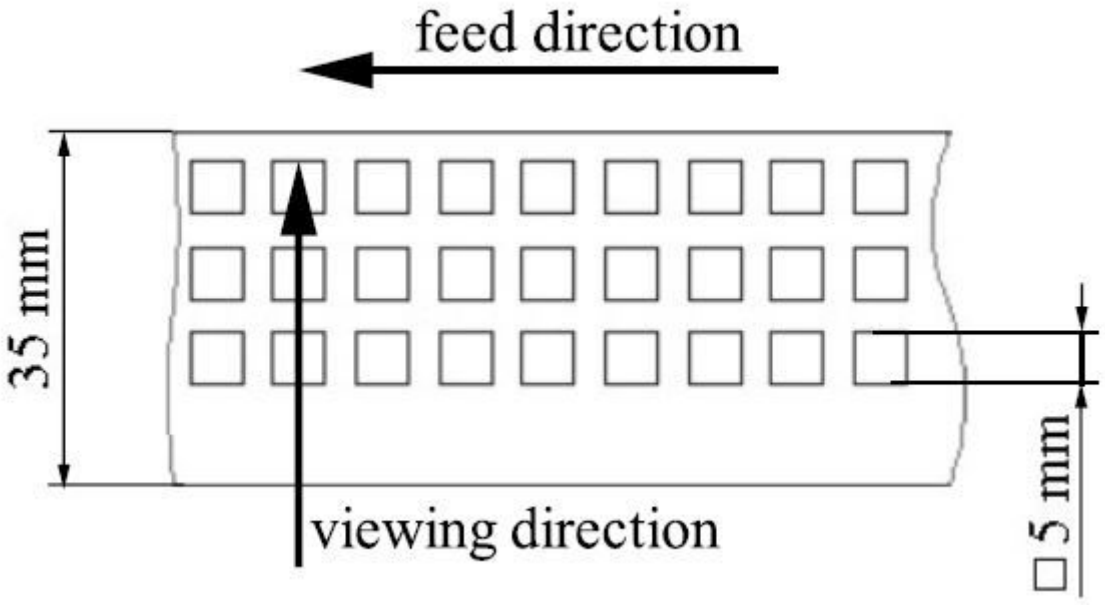

Figure 3

Simplified produced stamping part which was used to design and test the developed monitoring system

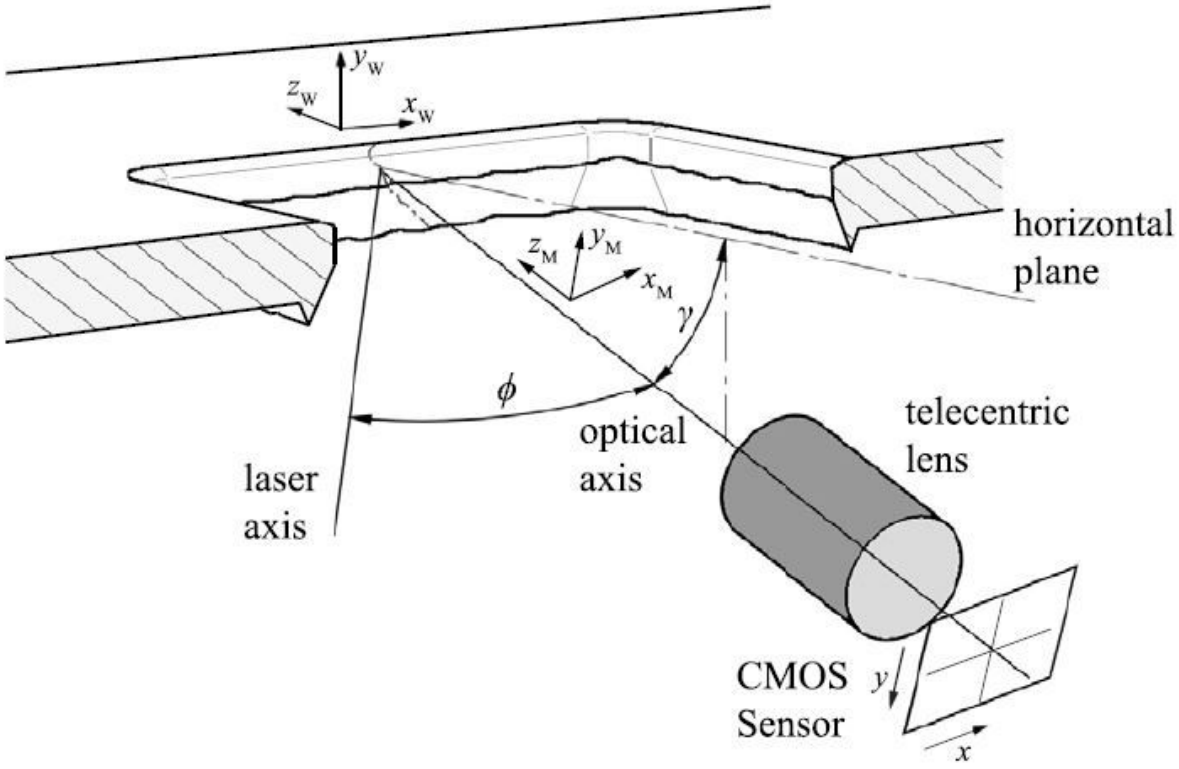

Figure 4

Imaging and triangulation setup with tilt angle γ and triangulation angle

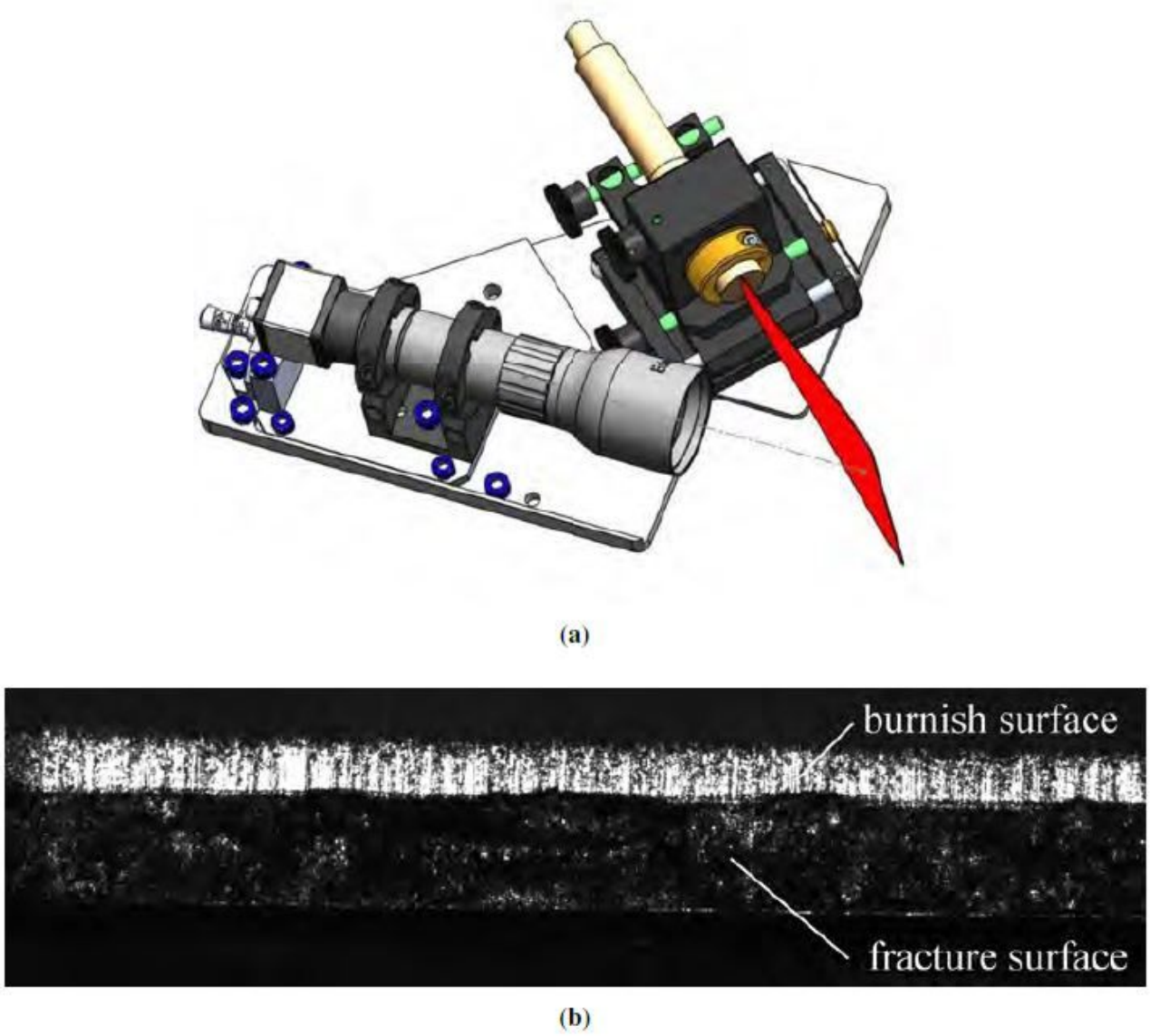

Figure 5

(a) Optical monitoring system with sensor, lens, laser mounted onto the baseplate (b) image of a cutting surface

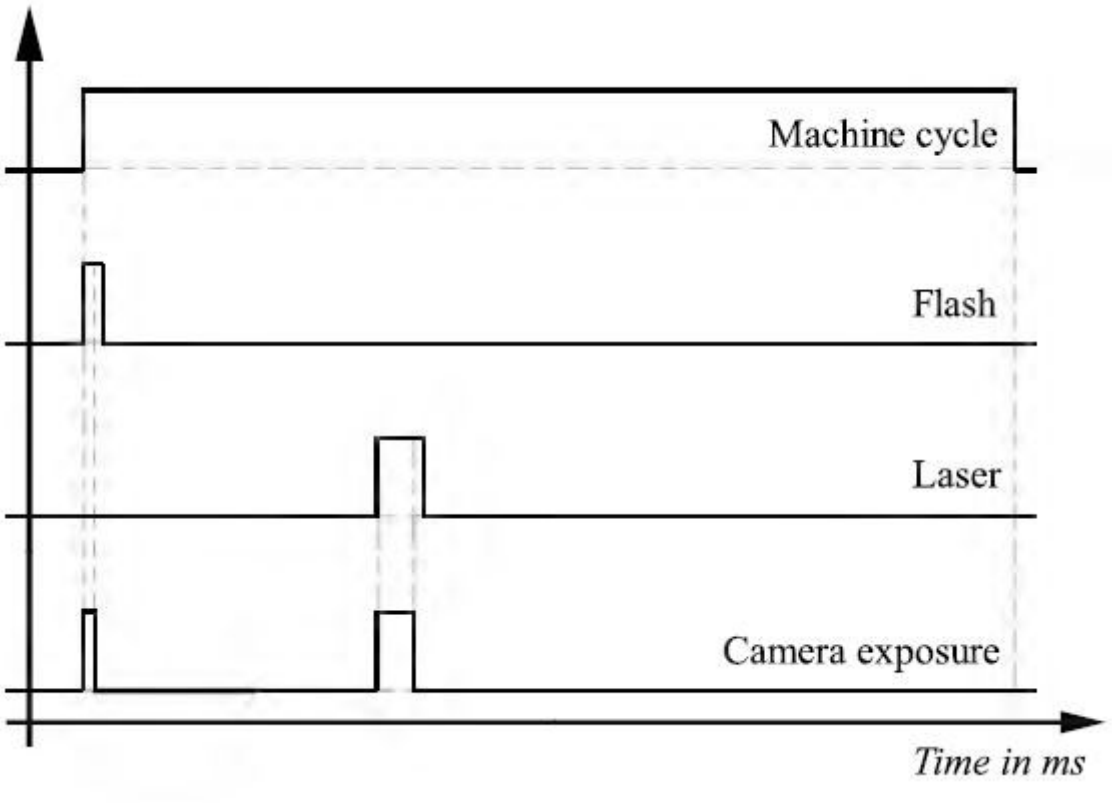

Figure 6

Workflow of the monitoring system

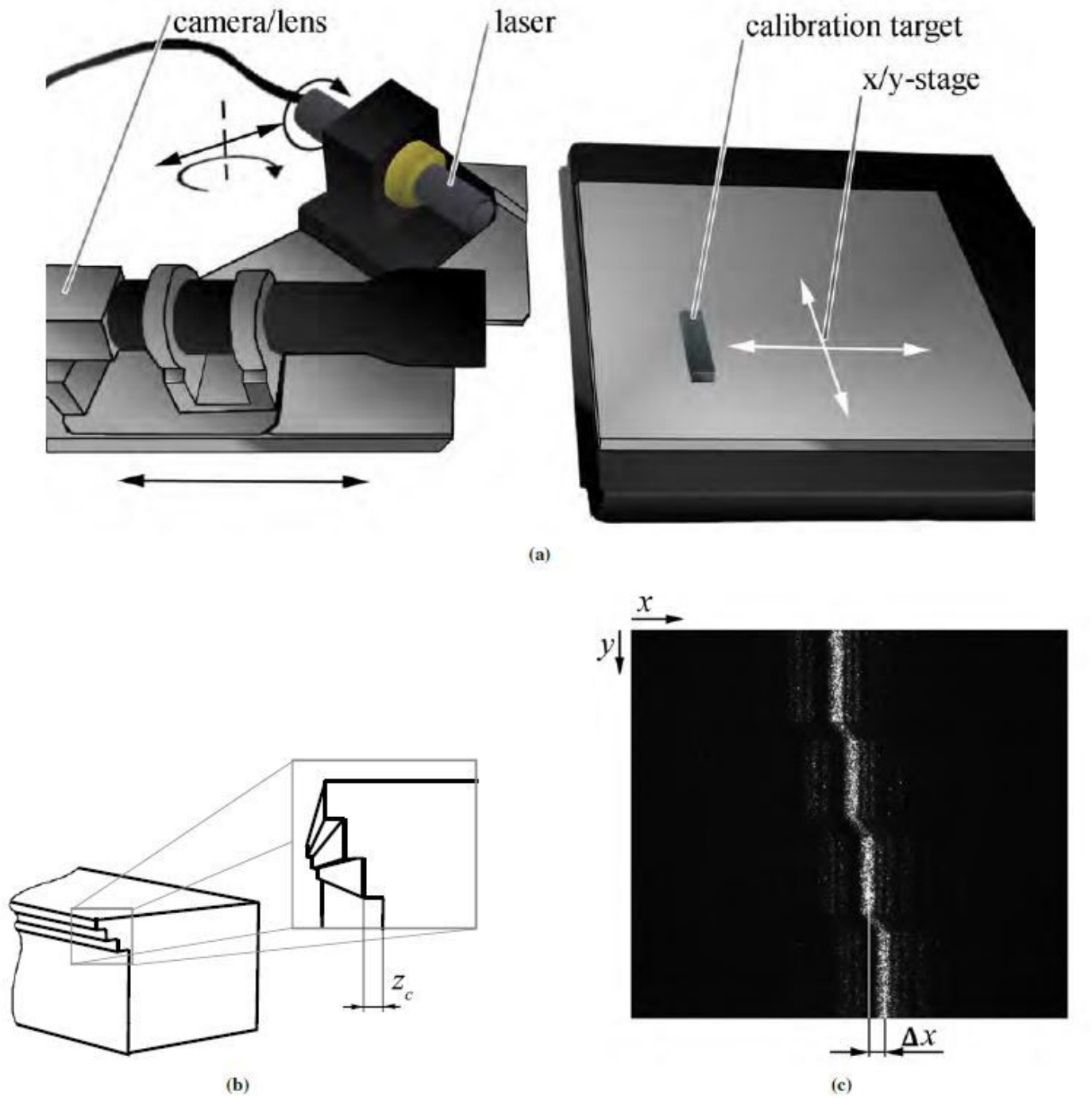

Figure 7

(a) Calibration setup (arrows depict degrees of freedom) (b) Calibration target (c) Calibration Image

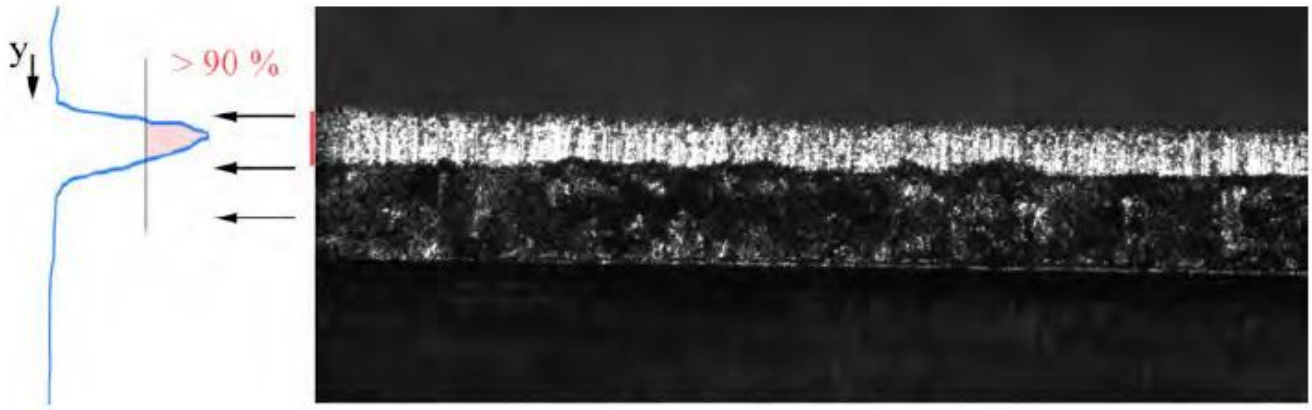

Figure 8

Rough selection of the burnish part for creation of the feature image

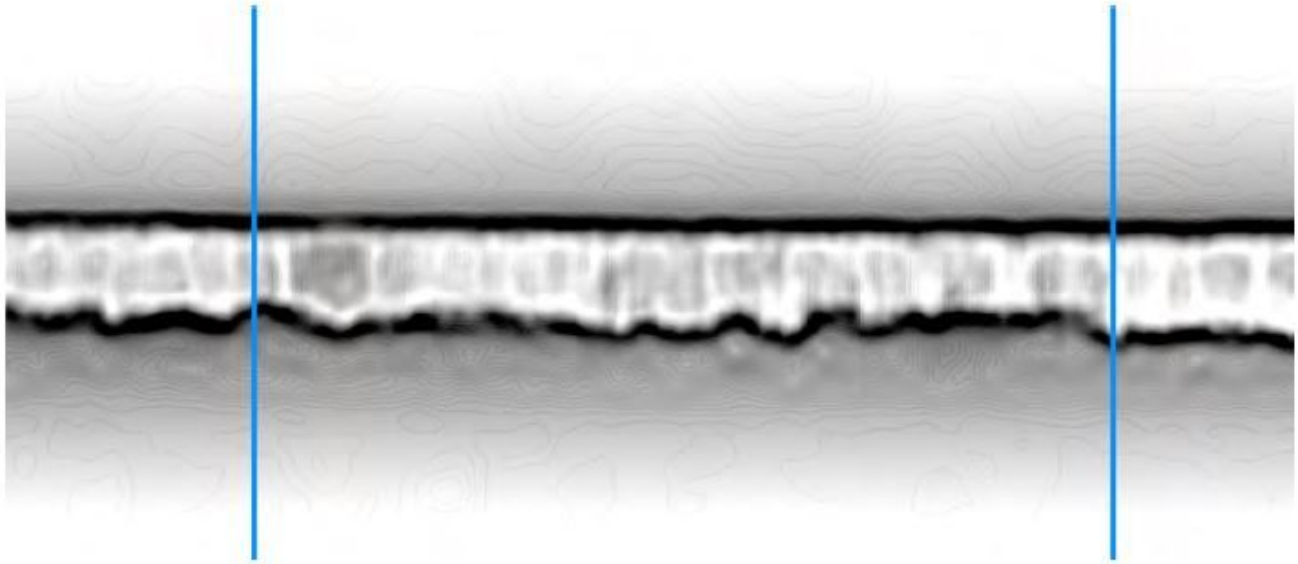

(a)

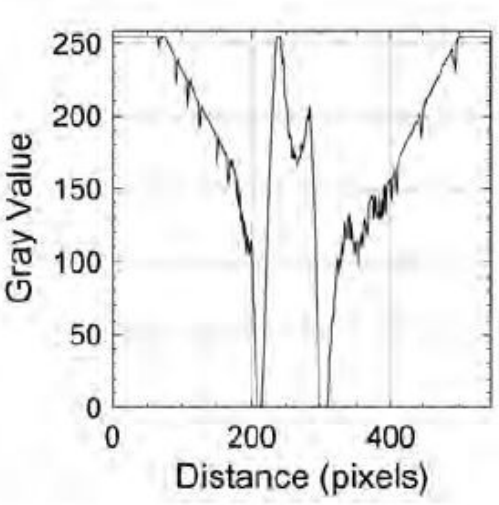

(b)

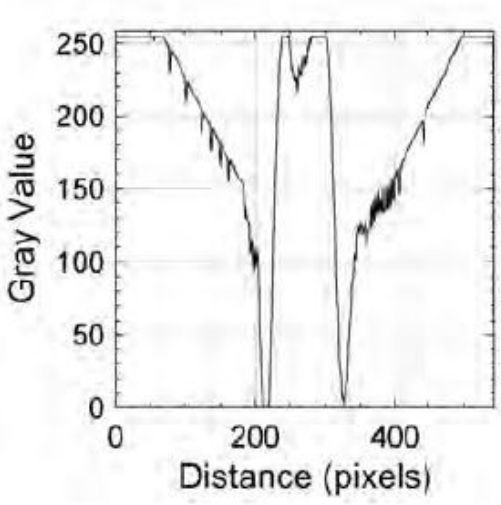

(c)

Figure 9

(a) Feature Image (b) Profile of the left vertical line (c) Profile of the right vertical line

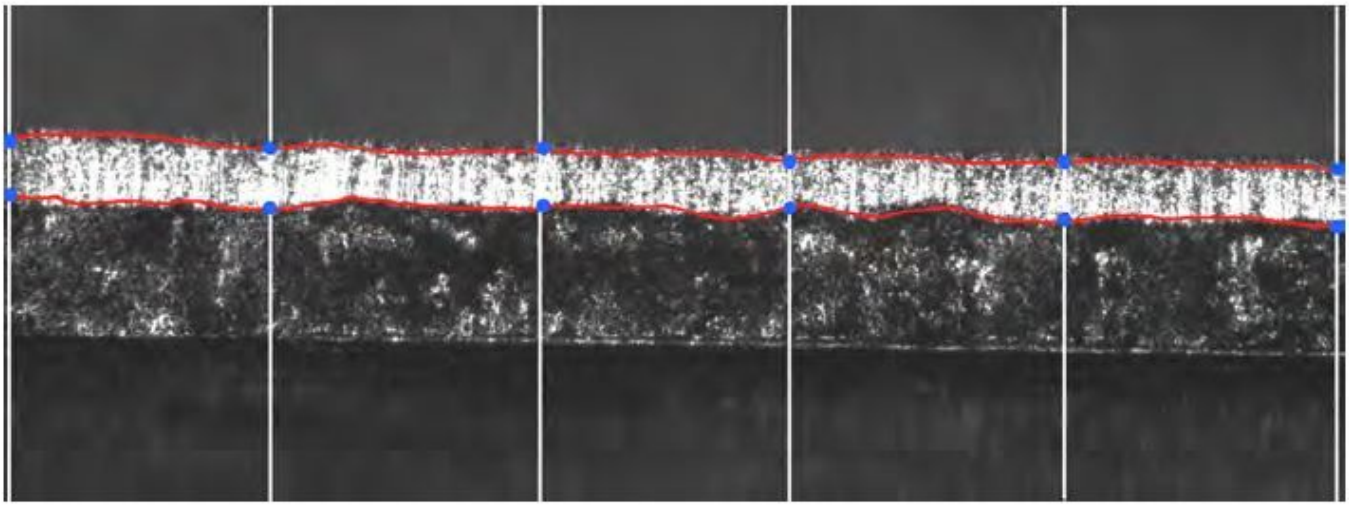

Figure 10

Segments for initial contour. Each segment performs a cumulative projection of the intensity along their length. The distance of the y-coordinates which are below yheight are picked and represented as the blue points. The red curves are calculated based on these points.

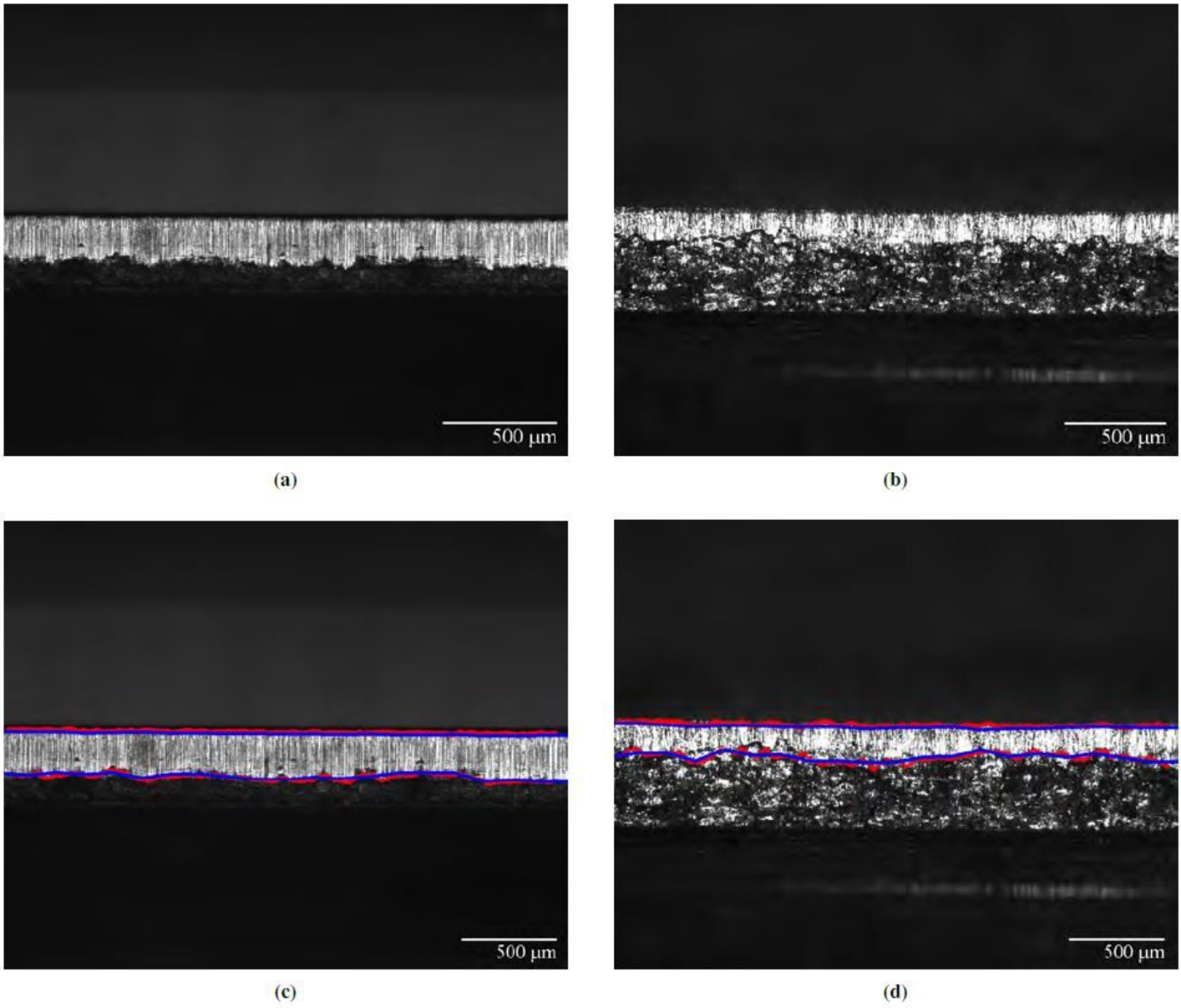

Figure 11

(a) image of stainless steel (b) image of copper (c) segmentation of image a (d) segmentation of image blue line = initial contour, red line = segmentation

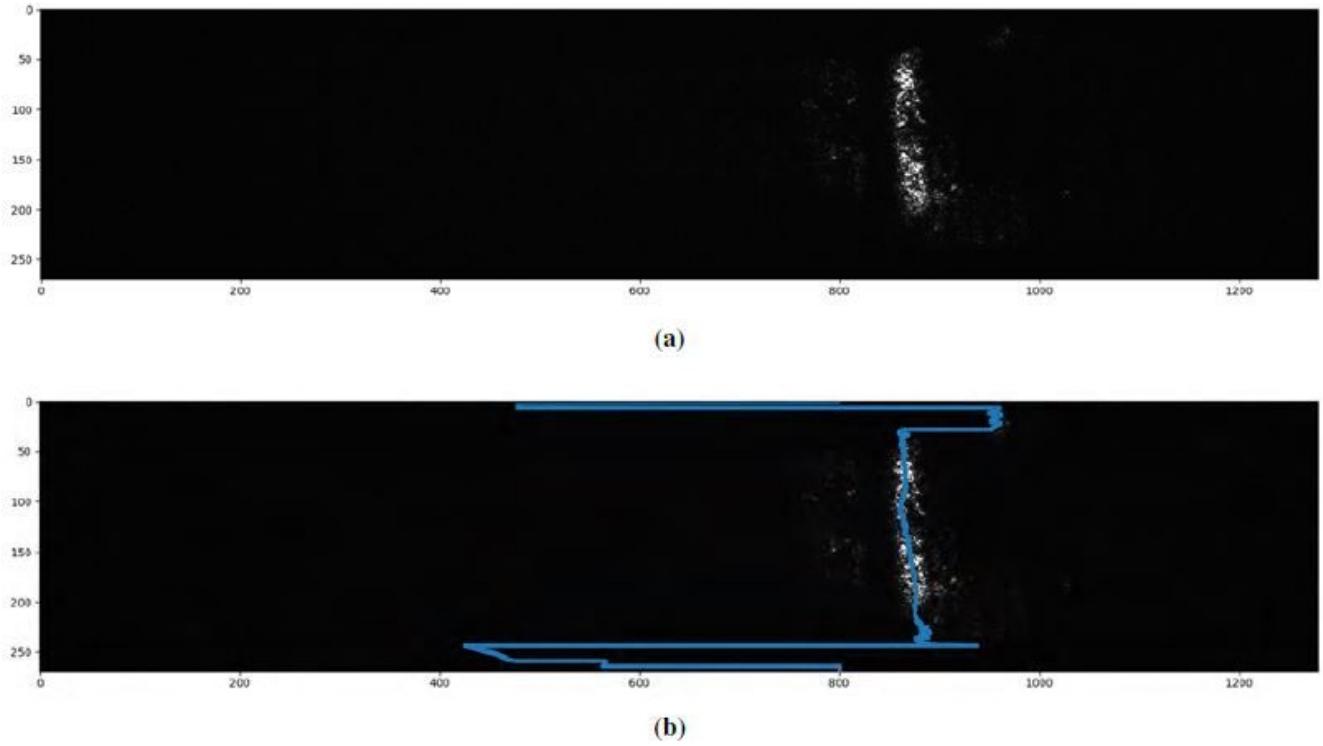

Figure 12

(a) triangulation image (b) segmentation of the triangulation image

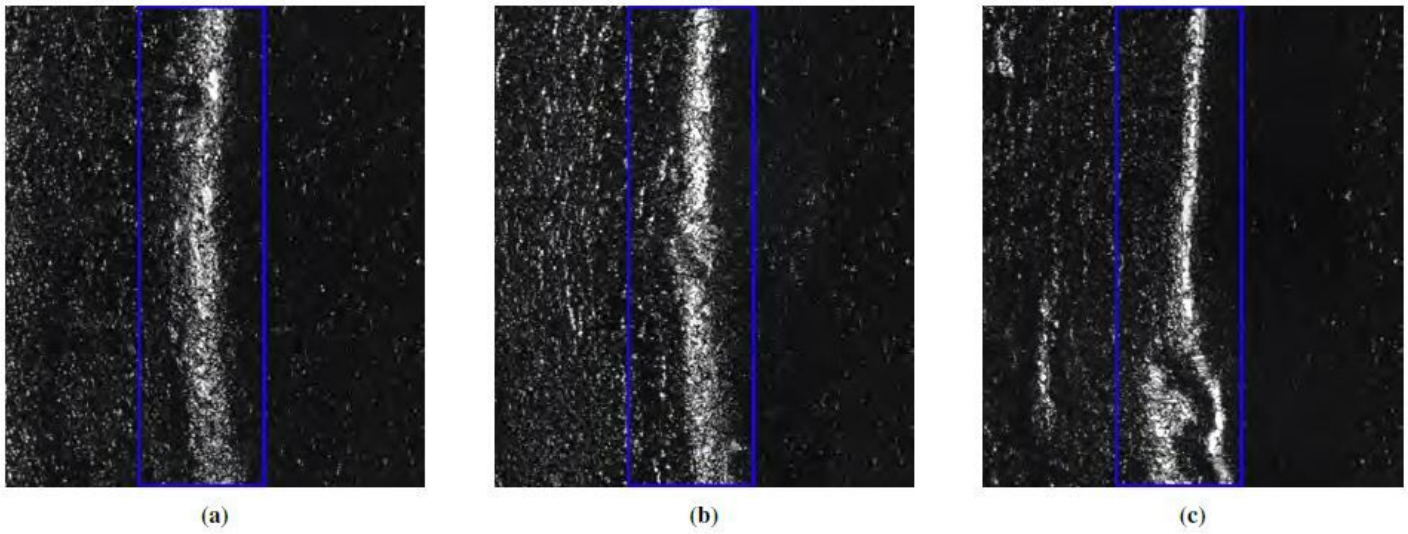

Figure 13

Confocal microscope images of the cutting edge (highlighted blue box) of the punch (a) cutting edge (punch) 5.000 strokes (b) cutting edge (punch) 10.000 strokes (c) worn out cutting edge (punch) 25.000 strokes

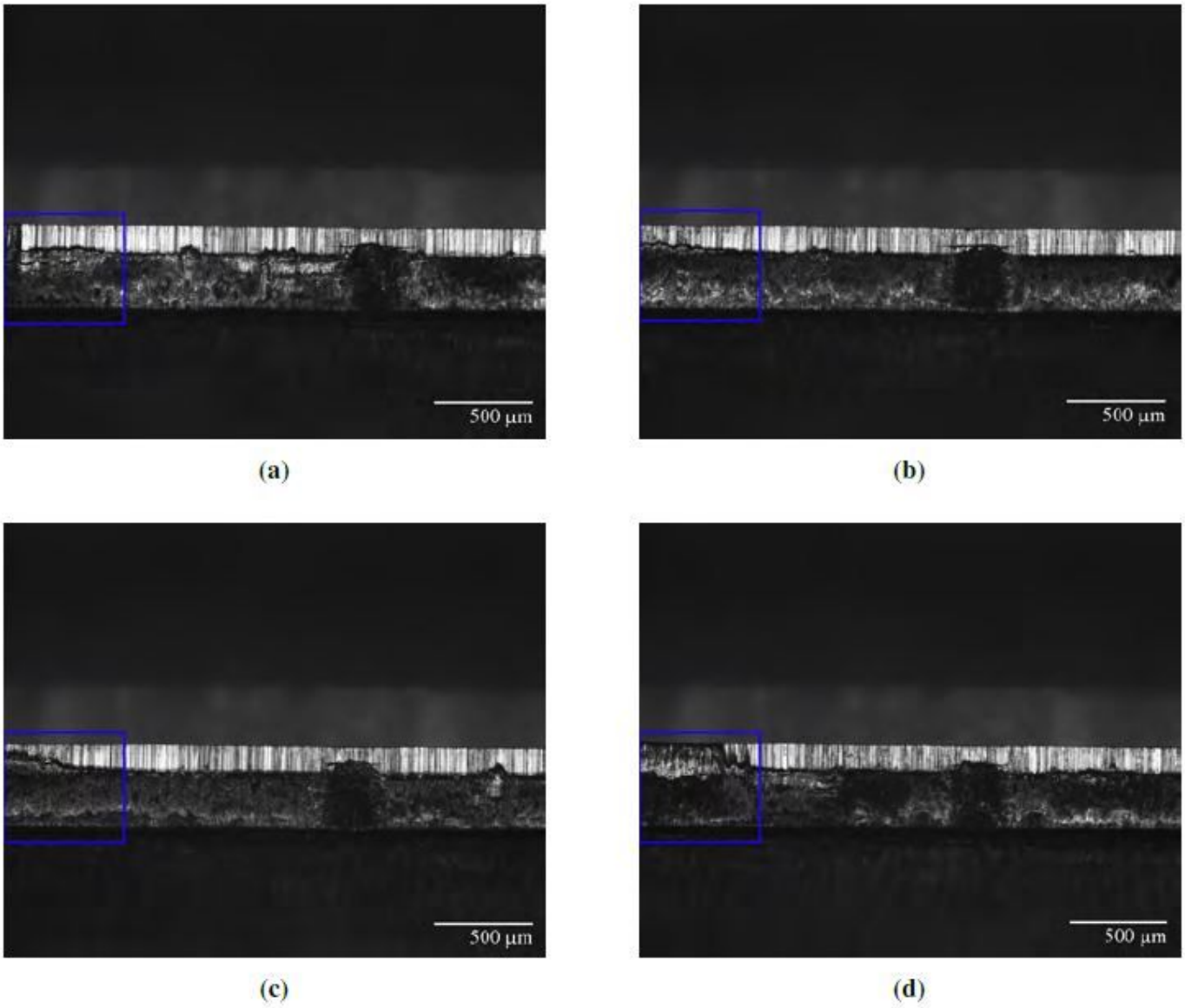

Figure 14

(a) cutting surface 10.000 strokes (b) cutting surface 13.000 Strokes (c) cutting surface 13.500 strokes (d) cutting surface 25.000 strokes

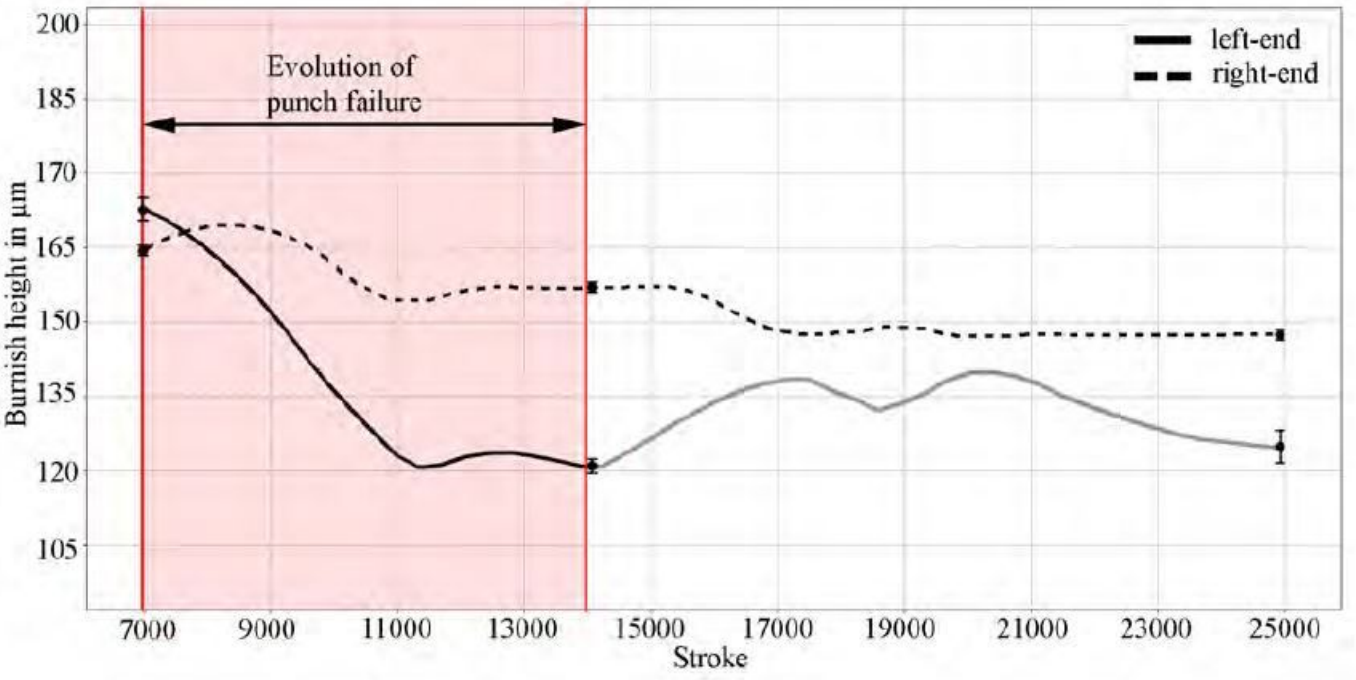

Figure 15

Diagram of the burnish height at the left-and right-end of the Image

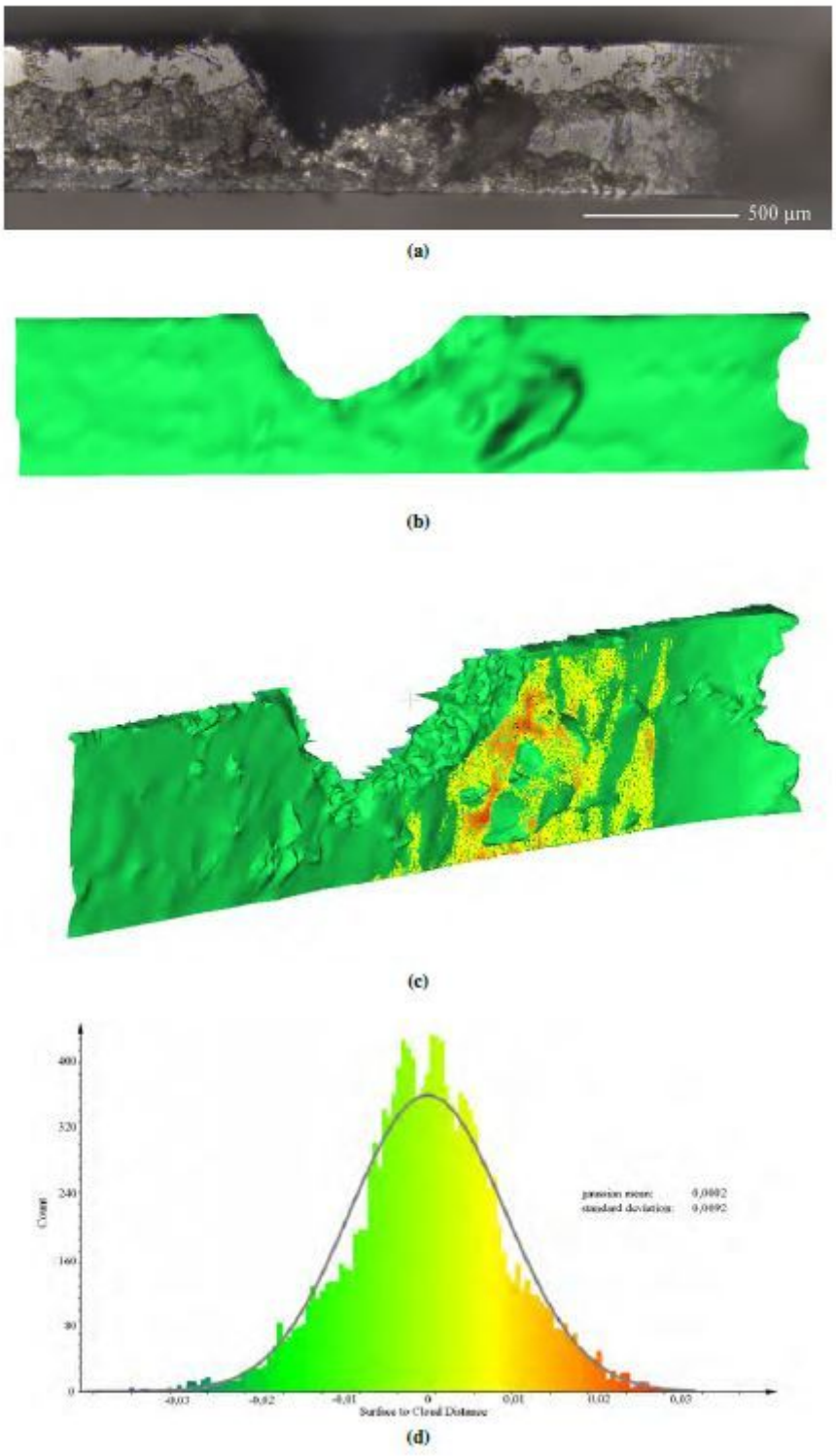

Figure 16

Part 1 (a) microscope image (b) surface from microscope (c) surface to cloud distance with aligned cloud (d) histogram of surface to cloud distance distribution

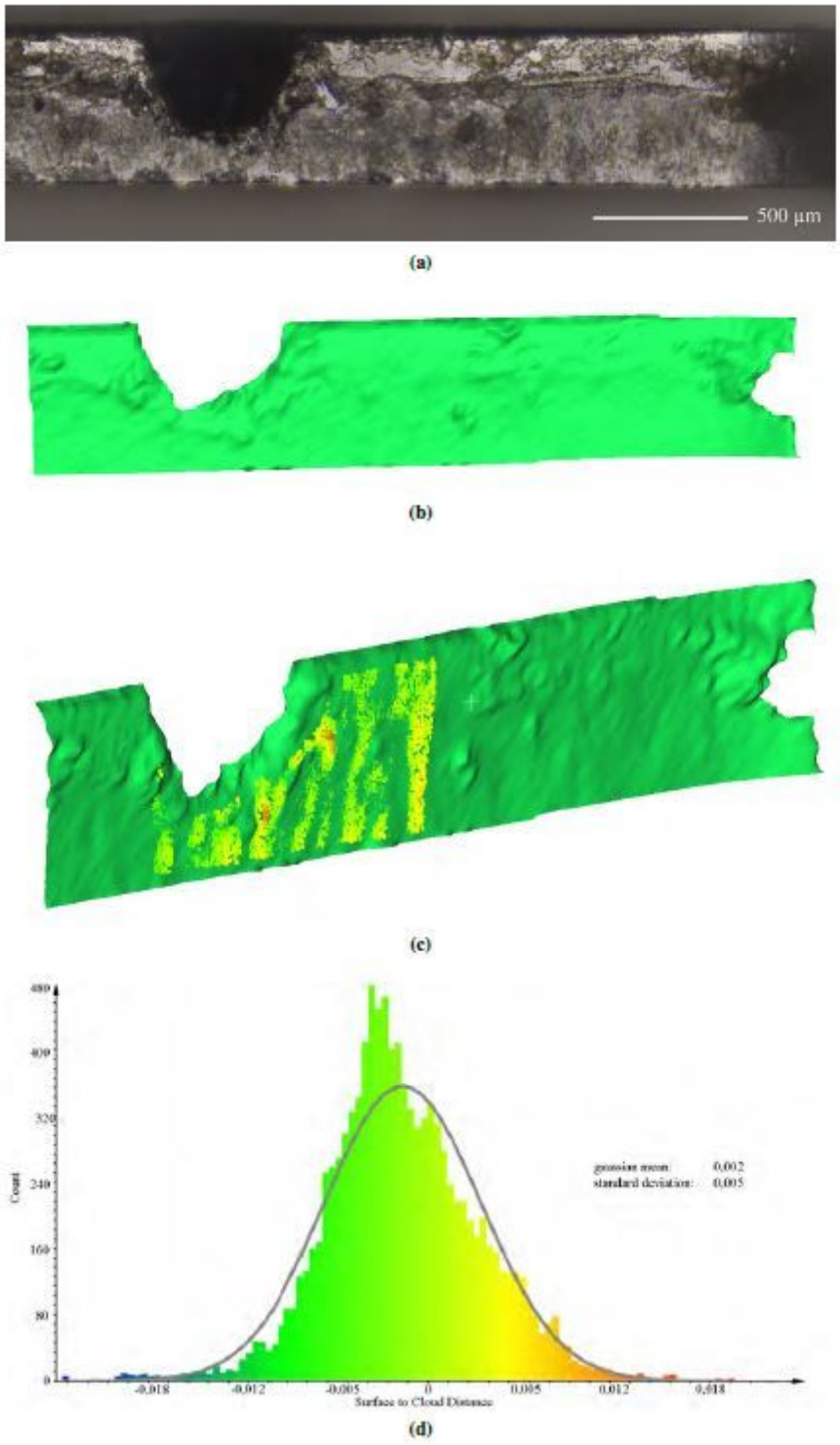

Figure 17

Part 2 (a) microscope image (b) surface from microscope (c) surface to cloud distance with aligned cloud (d) histogram of surface to cloud distance distribution

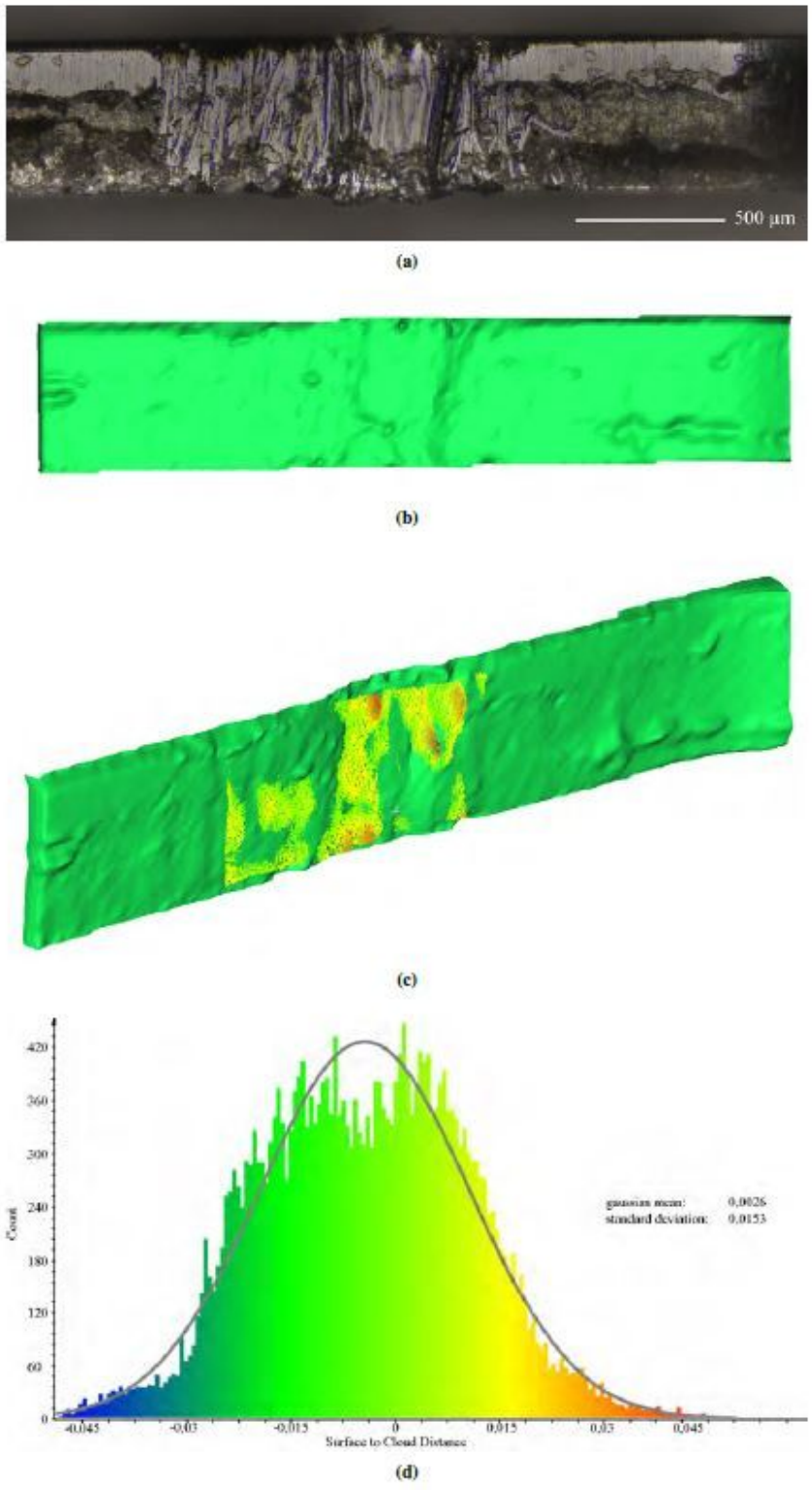

Figure 18

Part 3 (a) microscope image (b) surface from microscope (c) surface to cloud distance with aligned cloud (d) histogram of surface to cloud distance distribution